SYNTHESIS AND CHARACTERIZATION OF IRON OXIDE VIA CHEMICAL LEACHING FROM BIOINSPIRED TERMITE MOUND FOR BIOMEDICAL APPLICATION

A Thesis Submitted to the School of Graduate Studies,

African University of Science and Technology, Abuja, Nigeria

In Fulfillment of the Requirements for the

Degree of Master of Science in Materials Science and Engineering

By:

THOMAS CHETU BEWAALE

SUPERVISOR: DR. DANYUO YIPORO

MARCH 2021

CERTIFICATION

This is to certify that the thesis titled "**Synthesis and Characterization of Iron Oxide Via Chemical Leaching from Bioinspired Termite Mound for Biomedical Application**" submitted to the school of postgraduate studies, African University of Science and Technology (AUST), Abuja, Nigeria for the award of Master's degree, is a record of original research carried out by Thomas Chetu Bewaale in the Department of Materials Science and Engineering.

Thomas Chetu Bewaale (ID: 40727)

Signature: …… 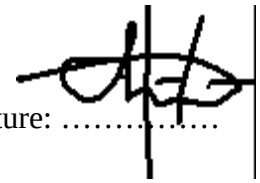 Date: 11th March 2021.

SYNTHESIS AND CHARACTERIZATION OF IRON OXIDE VIA CHEMICAL LEACHING FROM BIOINSPIRED TERMITE MOUND FOR BIOMEDICAL APPLICATION

By:

Thomas Chetu Bewaale

A THESIS APPROVED BY THE MATERIALS SCIENCE AND ENGINEERING DEPARTMENT

RECOMMENDED: --  ----------

Supervisor, Dr. Danyuo Yiporo (Date: 15/04/2021)

Head, Department of Materials Science and Engineering

(Professor Azikiwe Peter Onwualu, FAS)

APPROVED: ----------

Chief Academic Officer

Date:

©2021

Thomas Chetu Bewaale

ALL RIGHTS RESERVED

ABSTRACT

Nanomedicine has gained a lot of attention as a potential solution in theragnosis of cancer. With the introduction of nanoscale metallic oxide materials, imaging techniques, disease detection, and treatment modalities could be enhanced. The health benefits of particles in applications such as cancer treatment have greatly motivated the extraction of iron oxide from a local source such as from bioinspired termite mound, to enhance localized hyperthermia treatment via laser application or by the use of magnetic resonance imaging (MRI). The clay ore obtained from the termite mound was ground and mechanically sieved to $45\,\mu m$. This size range provides large surface areas for the leaching process. A phosphoric acid solution at varying molarity (0.1 M, 0.5 M, 1.0 M, and 3.0 M) was employed to leach iron oxide from a clay mineral at $100\,℃$. Elemental analysis using Energy Dispersive X-ray Spectroscopy (EDS) showed the raw clay initially contained 16.8% of iron content and was reduced to 2.27% after leaching with phosphoric acid. The functional group of the raw material was investigated with Fourier transform infrared radiation (FTIR) Spectroscopy. The UV/Vis spectroscopy technique was used to determine the presence of iron oxide within an absorbance range of 350-600 nm. Kinetics of the iron leaching process was also presented. Result agreed with previous studies on iron extraction using chemical means.

Keywords: Iron oxide, chemical leaching, leaching kinetics, Energy Dispersive X-ray Spectroscopy (EDS), Fourier Transform Infrared Radiation (FT-IR) Spectroscopy and UV/Vis Spectroscopy analysis.

DEDICATION

This thesis is dedicated to my parents (late mother, Bezaa-inibe Dooh and father, Paabang Kuuwmew), the entire Naabo and Bewaale families for their loving support and encouragement.

ACKNOWLEDGEMENTS

All praise be to the Father Almighty for the privilege, gift of life, and strength toward my academic work.

I am very grateful to the African Development Bank (AfDB), the Pan African Materials Institute (PAMI), and the African University of Science and Technology, Abuja-Nigeria for the scholarships during my studies.

My gratitude is extended to Dr Danyuo Yiporo for his mentorship, guidance, and usual support.

My sincere gratitude also goes to my Co-Supervisor, Dr Odusanya Shola for his assistance in the lab.

Appreciation is also extended to Prof. Wole Winston Soboyejo and Prof. A. P. Onwualu (HoD, Materials Science and Engineering), my thesis advisers, for their incredible support.

I must thank all those who worked with me on this project, specifically, Dr Bello Abdulhakeem, Dr Anye Vitalis, Theresa Ezenwafor, Anthony Elechi and Josephine Cee Udochukwu-Oparah.

My gratitude further goes to my friends, students, staff and professors, at the African University of Science and Technology, Abuja-Nigeria.

TABLE OF CONTENTS

List of Tables

List of Figures

CHAPTER ONE

1.0 INTRODUCTION

1.1 Background Studies

Cancer remains one of the major causes of morbidity and mortality in the world **[1, 2**]. In spite of the enormity of the problem, cost-effective detection and treatment options remain elusive and most often beyond the reach of the poor majority **[3]**.

Over 80% of African health care systems are inadequate in providing accurate theragnostic on cancer due to the low level of knowledge in biomaterials for health solutions **[2]**. Most communities in Africa resort to local herbs for cancer treatment. These herbs may impede cancer cells growth for some time but cancerous cells could regenerate.

The field of Nanotechnology in Medicine mirrors our next generation of cancer detection and treatment. Bioinspired research stands as an ever-growing field of endeavour in a wide range of biomedical application **[2,3]**. Bioinspired termite mould, a clay mineral contains characteristic iron oxide. Due to the activities of termites, most termitaria are clay in nature, smelled with precious minerals such as iron, gold, major and minor oxides **[4]**. Characterizing and synthesizing the iron oxide from termites mound would be studied in this work for biomedical applications.

Clay minerals are a group of phyllosilicate mineral which are characterized by their layered structure. Clay deposit constitutes one-third of the total soil surface. Because of their abundance, they have proven to be among the most important minerals in the industry due to their outstanding physical/chemical properties and are used in several applications, such as biomedical, ceramics, construction, and improving chemical

environments **[5].** In Africa, clay minerals are found in several places in the soil and its horizons. The geographical source and method of soil formation determine the significant iron content of the clay. An example of such ore is the banded iron formation. They are either alluvial or residual source formed as a result of volcanic deposits, rock dissolution, sedimentation, erosion, and under certain geological conditions. Clay minerals are normally located a few meters beneath the humus **[5, 6],** hence majority of termite mould contains iron oxide. Clay Minerals are amorphous with major oxides of $SiO_4 \wedge Al_2O_3$. They have a repeating tetrahedral and octahedral planar sheet **[5, 7]**. Through the activities of weathering and volcanic, minerals such as feldspar, quartz, mica, and iron are impacted onto the clay which changes its physicochemical properties. Clay contains organic matter such as lignite, colloidal minerals and iron which gives its colour, plasticity, and other desirable properties **[8, 9]**.

Natural existing clay deposit is whitish. When iron is in the lattice of the clay material, a low concentration of it may not impact any colouration **[6, 8]**. However, the presences of iron ore change its colour to reddish, for example $Fe^{2+¿¿}$converts to $Fe^{3+¿¿}$ through oxidation in the soil can confer colouration in the clay **[5, 10]**. Approximately, 0.4 %iron ore is enough to change its colour thus, reducing the refractory behaviour of clay deposits **[11].** For instance, red clay contains ironic oxide “minerals such as hematite (Fe_2O_3)”, “magnetite (Fe_3O_4)”, and “amorphous hydrated oxides” such as goethite ($\alpha - FeOOH$) and lepidocrocite ($\gamma - FeOOH$) **[9, 12].**

Iron oxide is the next abundance mineral in clay mineral apart from its structure component (silica and alumina) **[5].** There are several mechanisms used in the beneficiation of iron oxides from clay ore. These are categorized into physical and

chemical beneficiation process. In this study, the chemical beneficiation process shall be explored, since it gives much output of iron oxide. The diffusion of iron in water is extremely low but faster using strong acids. This includes leaching with chemical agents such as phosphoric **[9, 13]** or oxalic acid **[14–18]**. Leaching with "organic acids in the presence of a fermented medium", and bio-leaching was also explored in previous studies **[19]**. All these processes are geared towards removing the iron content from clay ore. Phosphoric acid has proven to enhanced a better yield of iron (98.65%) as compared to other organic leaching reagents **[9].** It has a lower activation energy of 10.18 kJ/mol which facilitate a chemical reaction **[9]**.

The removal of iron with phosphoric acid at different concentrations (0.1, 0.5, 1.0 and 3.0 M) was studied **[9].** It was demonstrated that increasing phosphoric acid content increased the dissolution of iron oxides into the solution. The leaching of iron oxides from clay through the product layer is enhanced by rate diffusion. The effect of temperature and particle size was studied. Decreasing the particle size of the clay mineral from $45\,\mu m$ increase the iron concentration in the gangue **[9].**

1.2 Problem statement

Africa is endowed with numerous natural resources. Most of them include iron, barite, gold, etc. However, most of the resources are mined by foreign nationals. The direct economic benefits from mining are, therefore, not realized since greater sums of money is lost in the process. Also, due to technical know-how, most of the youth are unemployed on the continent. Mineral processing and materials realization have been limited in most African industry. Clay has been extensively used in the production of pots

and other industrial activities in most African countries. Clay minerals from bioinspired-termite mound have not been extensively exploited in Africa for mineral extraction and beneficiation. This research shall explore innovative methods for iron oxide beneficiation.

Various materials have been engineered for biomedical applications due to their biocompatibility. Nano-sized materials have gained a lot of scientific focus in application to cancer treatment, target drug delivery and as contrast media**.** The extraction of iron oxide from clay is important for diverse applications.

The advocate for the Green chemistry approach has attracted the attention of researchers to find out the non-toxic method for synthesizing/beneficiating iron oxide particles.

Additionally, major cancer treatment involves surgery or radiotherapy. Surgery may not remove the entire lump (cancerous cells) which may cause regeneration of cancer. Second-time surgery is barely impossible or it leaves the patient incapacitated. Radiotherapy is another method of cancer treatment but due to excessive radiation other associated cells may die living the patient impaired hence there is the need for safer treatment procedures.

The focus of this work is on the characterization of clay ore and the extraction of iron for biomedical application.

1.3 Motivation

The production and synthesis of iron oxide may require the use of several reported approaches many of which employ the use of expensive yet toxic chemicals

which lead to the formation of hazardous by-products and contamination from precursor chemicals used. Mimicking nature to our benefits is the underlying motivation of this work. We explore termitarium since they are dominant in most African countries. Bioinspired termite mound could be a source of mineral deposit. Iron oxide could be synthesis via leaching experiment for biomedical application.

1.4 Justification

Nanotechnology is the hallmark of our fourth industrial revolution. The ability to manipulate materials to fill ones Socioeconomic needs drives the development and advancement of that society. The rapid growth of nanotechnology in Medicine offers improvement in cancer theragnostic due to the introduction of IONPs. These IONPs in their applications have usually composed of a magnetic core engulfed with various functional groups aiding them in hyperthermia treatment, magnetic resonance imaging (MRI), optical imaging, biosensor, and cell separation **[3-9**]. These IONPs can be directed to particular cancer sites for drug delivery using external magnetics in cancer treatment. Also, in the detection of cancer growth, they can be scanned with MRI's when developed and designed by embedding them with receptors that are attracted to the cancer cell. When synthesized and functionalized, they have shown potential therapeutic effects on cancer cells.

Different methods have been explored in synthesizing iron oxide nanoparticles such as the use of ferric chloride ($Fe_3Cl.6H_2O$), ferric sulphate ($FeSO_4.7H_2O$), hydrochloric acid (HCl), and ammonium hydroxide (NH_4OH) acid solutions. Studies on synthesizing iron oxide particle from a bioinspired termite mound are limited hence the

need to conduct this research. The current work shall focus on characterizing and chemical leaching of iron oxide particles from a bioinspired termite mound obtained from SHETSCO, the Federal Capital Territory of Nigeria, Abuja.

The cost involved and the environmental challenges imposed by the current method of iron oxide particles synthesis indicate the need for a safer approach. The use of a bioinspired termite mound to obtained these particles without mixing so many chemicals are the basis for this research. This will remedy the problems caused by the former procedures.

1.5 Goal of Project

Synthesis and Characterization of iron oxide particles (IONPs) from a bioinspired termite mound via chemical leaching with phosphoric acid for biomedical application in cancer detection and treatment.

1.6 Specific Objectives

- Morphological characteristics of the clay mineral with “Scanning Electron Microscopy (SEM) and EDS” to analyse the percentage elemental composition.
- Effect of comminution and iron oxide concentration during the beneficiating process.
- Functional group determination of the clay ore and ore residue with Fourier Transform Infrared Radiation (FT-IR) Spectroscopy.
- Using low energy process via recommended chemical acids (phosphoric Acid solution) for the processing of iron concentrates from the clay mineral.

- Study the kinetics of chemical synthesis at known acid concentrations (time and temperature effects).

Reference

[1] WHO, “Cancer, Regional Office for Africa.” https://www.afro.who.int/health-topics/cancer (accessed Jan. 27, 2021).

[2] K. H. Bae, H. J. Chung, and T. G. Park, “Nanomaterials for cancer therapy and imaging,” *Mol. Cells*, vol. 31, no. 4, pp. 295–302, 2011. DOI: 10.1007/s10059-011-0051-5.

[3] Amarkai A., Efavi J., Tiburu E.K., “Biosynthesis of Magnetite iron oxide Nanoparticles and its Potential Application for Cancer Treatment, vol. 10, no. 2, pp. 1–15, 2018.

[4] E. Arhin and P. M. Nude, “Use of termitaria in surficial geochemical surveys : Evidence for > 125- μ m size fractions as the appropriate media for gold exploration in northern Ghana Geochemistry : "Exploration, Environment, Analysis Use of termitaria in a surficial geochemical survey,” 2010. DOI: 10.1144/1467-7873/09-004.

[5] R. B. Asamoah *et al.*, “Industrial applications of clay materials from Ghana (a review),” *Orient. J. Chem.*, vol. 34, no. 4, pp. 1719–1734, 2018. DOI: 10.13005/ojc/340403.

[6] A. A. J. Kesse, G. O.; Balkema, “Water Resource and Protection,” j*ournal Water Resour. Prot.*, no. 1(3), pp. 522-530, 1996.

[7] C. D. Pavlidou, S.; Papaspyrides, “Progress in polymer science,” *Prog. Polym. Sci.*, no. 33(12), pp. 1119–98, 2000.

[8] E. E. Norton, F.H., Robert, “‘Fine Ceramics: Technology and Applications,’” *Krieger Publ. Co., vol. New York*, p. 1978.

[9] U. P. Acid, “Kinetics of Iron Leaching from Kaolinitic Clay, Using Phosphoric Acid” 2016. DOI: 10.3390/min6030060.

[10] M. MacEwan, D. M.; Wilson, “Soil Science,” *J. Soil Sci. Soc. Am.*, vol. 5, pp. 197-248, 2018.

[11] A. Tuncuk and A. Akcil, “‘Removal of iron from quartz ore using different acids:

A laboratory-scale reactor study,’ Miner Process..,” *Extr. Met. Rev.*, vol. 35, no. 4, pp. 217–228, 2014.

[12] N. Taitel-Goldman, “‘Iron Oxides Synthesized in Hypersaline Solutions,’” *Miner. - Significance Appl.*, vol. 6, pp. 1–11, 2019.

[13] T. I. Zhang, Z.; Li, J.; Li, X.; Huang, H.; Zhou, L.; Xiong, “High-efficiency iron removal from quartz sand using phosphoric acid.,” *J. Miner. Process.*, vol. 114, pp. 30–34, 2015.

[14] P. F. M. Legorreta-García, F.L.; Cruz, L.E.H.; Muñoz, “Estudio de la remoción de impurezas de arcillas (México)., caoliníticas del estado de Hidalgo,” *Rev. Latinoam. Met. Mater.*, vol. 33, pp. 313–314, 1989.

[15] L. E. . J. Hernández, H.; García, F.L.; Hernández Cruz, “Kaolin bleaching by leaching using phosphoric acid solutions.,” *A.B. J. Mex. Chem. Soc.*, vol. 59, pp. 198–201, 1998

[16] A. Panias, D.; Taxiarchou, M.; Paspaliaris, I.; Kontopoulos, “Mechanisms of dissolution of iron oxides in aqueous oxalic acid solutions. Hydrometallurgy,” vol. 42, pp. 257–265, 2016.

[17] M. L. Aguilera, N.H.; Jackson, “Iron oxide removal from soils and clays.,” *Soil Sci. Soc. Am. J.*, vol. 17, p. 359, 2015.

[18] M. Ambikadevi, V.R.; Lalithambika, “Effect of organic acids on ferric iron removal from iron-stained kaolinite.,” *Appl. Clay Sci.*, vol. 16, pp. 133–145, 2002.

[19] and A. M. L. R. A. H. Hernández, F. L. García, L. E. H. Cruz, “‘Iron removal from a kaolinitic clay by leaching to obtain high whiteness index,’ vol. 45,” in *IOP Conf. Ser. Mater. Sci. Eng.*, p. no. 1, pp. 6–10, 1978.

‘

CHAPTER TWO

2.0 LITERATURE REVIEW

2.1 Introduction

GLOBOCAN 2020 report **[1–3]** estimated over 19.3 million new cancer cases and 10 million cancer deaths **[4, 5].** Based on the GLOBOCAN 2012 report, 57% of incidences and 65% of mortality are recorded globally **[2, 3]**.

In Africa, studies from GLOBOCAN 2020 shows that there are 6% of incidences and 7.2% mortality within the "54 countries of Africa, with about three quarters in the 47 countries of Sub-saharan Africa" **[3]**. The annual cancer incidences and mortalities are expected "to increase by at least 70% by 2030 globally", therefore a pressing need to improve on cancer detection and treatment **[3, 6]**.

Cancer in human is a disease caused by uncontrolled cell division, "genetic instability, accumulation of multiple molecular alterations" **[7–9],** and indecent lifestyle. For both sexes, lung cancer was the most frequently "diagnosed cancer (11.6% of total cases) and the leading cause of cancer death (18.4% of total cancer deaths), followed by breast cancer in women (11.6 %), colorectal cancer (10.2%) and prostate cancer" (7.1%) in terms of incidence. In terms of morbidity, "colorectal cancer (9.2%), stomach cancer (8.2%) and liver cancer" (8.2%) were reported among the above-mentioned mortality.

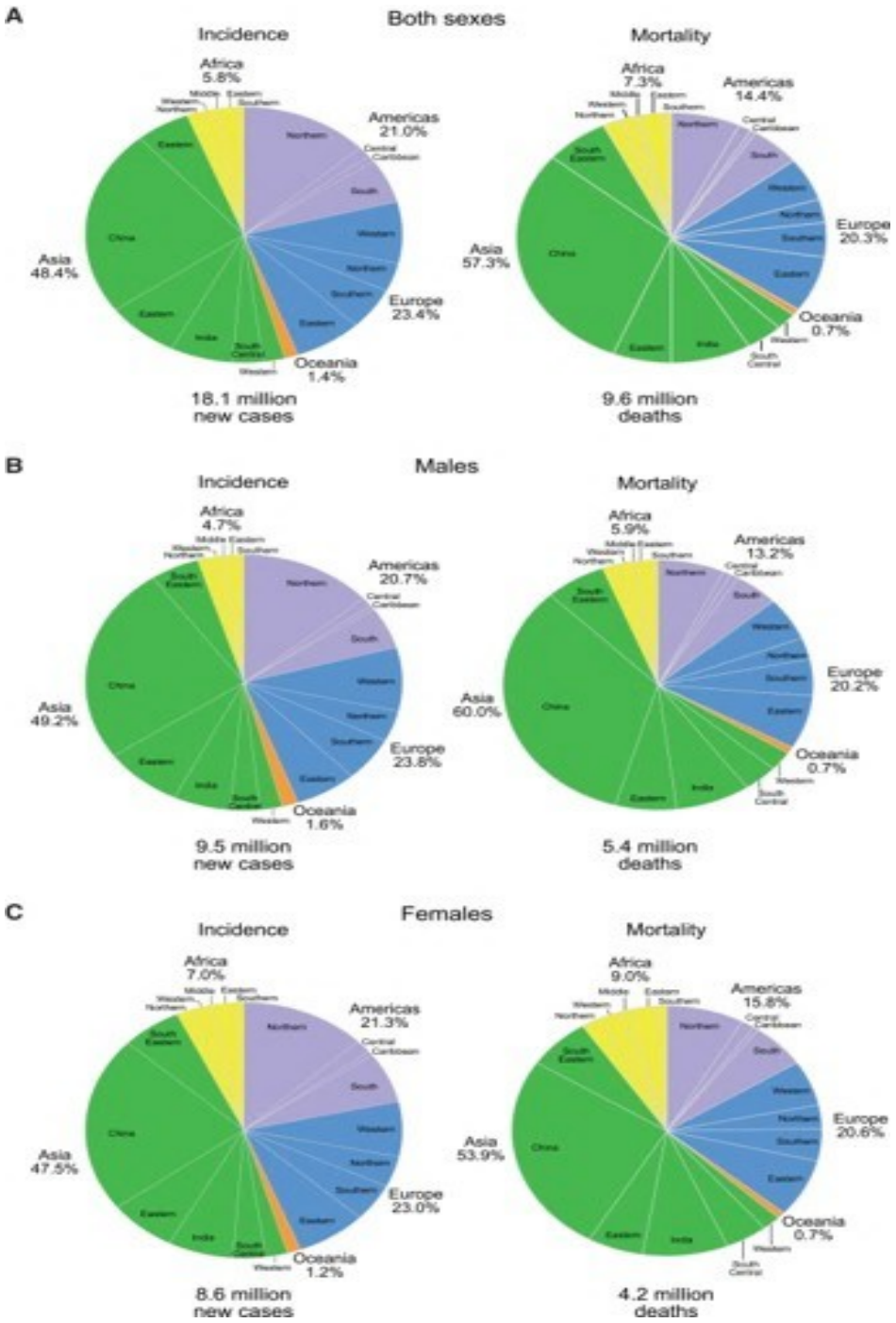

Figure 2.1: Pie charts show the distribution of cases and deaths by region in 2018 for (a) both sexes, (b) men, and (c) women. For each gender, the length of the pie chart represents the proportion of the total number of cases of illness or death. GLOBOCAN 2018 **[5]**.

Depending on gender, “lung cancer is the most commonly diagnosed cancer and the leading cause of cancer death in men” **[5]**, followed by prostate and colon and liver and stomach cancers. Among women, “breast cancer is the most commonly diagnosed cancer and the leading cause of death from cancer” **[5]**, followed by colon and lung cancer in frequency and vice versa in mortality; cervical cancer ranks fourth in morbidity and mortality. Overall, the top “10 cancers account for more than 65% of newly diagnosed cancers and deaths” **[5]**.

Figures 2.2 show the most frequently diagnosed cancer and the leading causes of mortality in men (**Fig. 2.2a**) and women (**Fig. 2.2b**). The maps reveal substantial global diversity in leading cancer types, particularly for incidence in males (10 different cancer types) and mortality in both men (9 types) and women (6 types).

In most African countries, cancer detection and treatment modalities are inefficient despite this increasing rate of cancer **[6]**. Current diagnostics and prognostics “classifications do not reflect the whole clinical heterogeneity of tumours and are insufficient to make predictions for successful treatment and patient outcome” **[7, 10, 11]**. Most current anti-cancer programs in Africa make little difference between cancer and normal cells, resulting in systemic toxicity and adverse effects. In addition, cancer is often diagnosed and treated very late if cancer cells have already invaded and metastasized to other parts of the body. Tumour cell detection is an important issue that has received widespread attention in recent years **[12]** for the identification of metastatic tumour cells with a special preference on both the “evolution of the disease and for the response of the patient to treatments”.

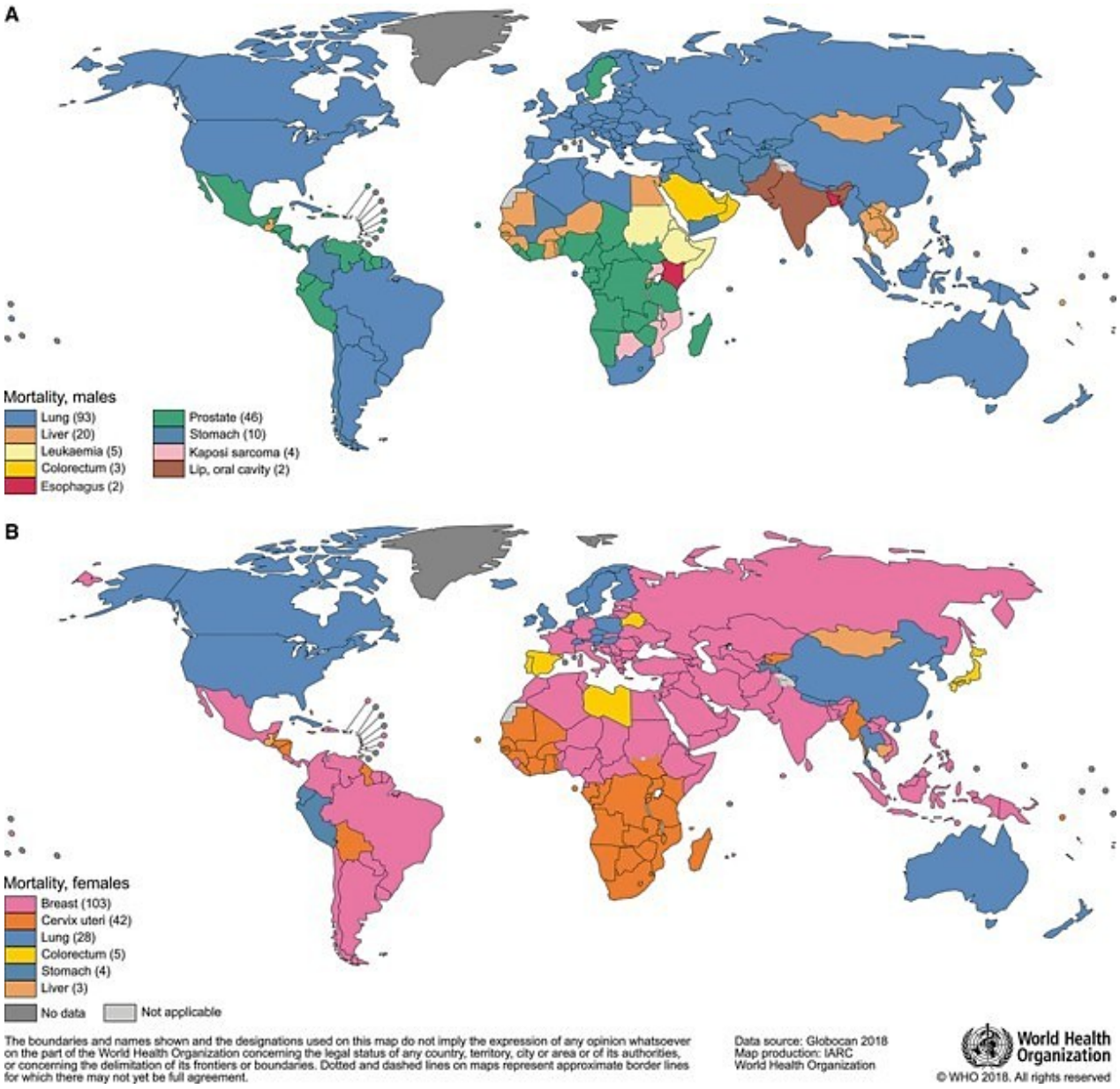

Figure 2.*2*:Global maps showing the most common types of cancer mortality by country in 2018 among (a) men and (b) women. The numbers of countries represented in each ranking group are included in the myth. Source: GLOBOCAN 2018 **[5]**.

Therefore, there is a high demand for “simple, efficient, rapid and user-friendly alternative methods for the detection and treatment of cancer amongst Africans” **[12].** Nanotechnology in cancer detection and treatment is an interdisciplinary field of research in science, technology and medicine, widely used for molecular imaging, molecular

diagnostics and targeted therapy. The basic idea is that nano-sized particles (metals, polymeric materials, semiconductors etc.) have unique properties such as electrical/electronics, “optical, magnetic, or structural that are not available from the bulk” solids macrometer **[13, 14]**. When functionalized with tumour “targeting ligands” such as Luteinizing Hormone-Releasing Hormone (LHRH), monoclonal antibodies, peptides, nucleic acids or small molecules **[15–22]**, “these nanoparticles can be used to target tumour antigens (biomarkers) and tumour vessels with high affinity and specificity”. Nanoparticles have large surfaces and functional groups for conjugation with multiple diagnostic (e.g., optical, radioisotope, or magnetic) and therapeutic (e.g., antitumor) agents (**Fig. 2.3**). Recent advances have led to research into bio-affinity nanoparticles for molecular and cellular imaging, targeted nanoparticles “for cancer treatment, and integrated nanodevices for early detection and screening of cancer”**[12]**. The “successful integration of nanoparticles into cell detection assays” could enhance the imaging of tumour cells **[12].**

The use of nanoparticles for drug delivery and targeting is probably one of the most interesting and clinically important applications of cancer nanotechnology. Iron oxide nanoparticles (IONPs) have also evolved in biomedical applications for cancer detection and treatment, such as the use of superparamagnetism as a contrast agent for the detection of lymph node prostate cancer **[23]** and the use of macromolecular nanoparticles for the delivery of drugs targeting the tumor vasculature **[24]**. “New technologies using metal and semiconductor nanoparticles are also under intense research and development for molecular profiling studies and multiplexed biological assays” **[25–29]**.

The goal of this work is to synthesis iron oxide from a bioinspired termite mound for biomedical application in the detection and treatment of cancer cells.

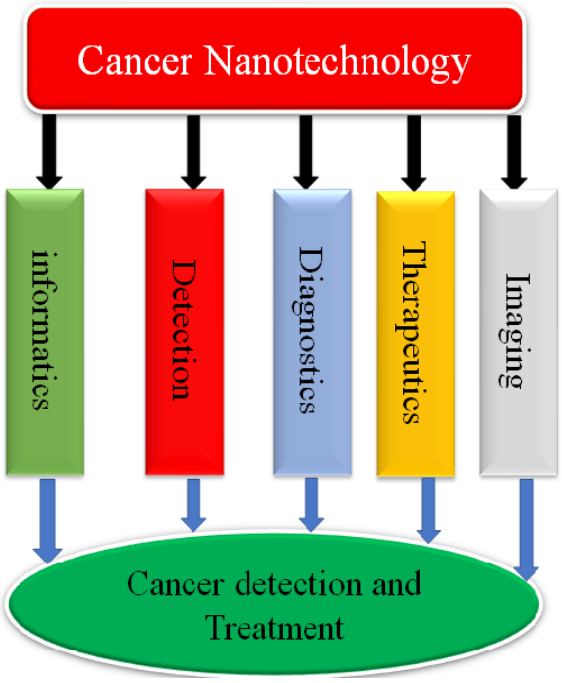

Figure 2.3: Schematic diagram showing the application of nanotechnology "in cancer through molecular tumor imaging, early detection, molecular diagnosis, targeted therapy and cancer bioinformatics" **[7]**.

2.2 Iron (Fe) deposit and Extraction in Africa

Iron (Fe) is one of the most abundant naturally occurring element in the earth's crust ranging from 2-3% in sedimentary rocks **[30]**, to 8.5% in igneous rocks **[31]**. It is a ferrous metal with enormous industrial benefits such as biomedical, paper clips, automobile bodies, and steel production **[50].**

Bioinspired termite mould can be used as a geographical factor in determining the location of precious metals **[33].** Mounds are characterized by a thick regolith and transported overburden of clay and precious minerals **[34].** Areas with thick regolith materials have been identified with mask bedrock mineralization **[33].** Studies show that

valuable minerals overlying bedrock is carried along by termite and mixed with fine regolith materials used in building the termitaria. This is an indication that bioinspired termitaria in most African countries could be used as a medium for sampling the mineral base of the region.

"Over time the termitaria may collapse and subsequently become eroded, transported and redeposited in lower beds" **[35]**. They may be residual or transported in nature. Research attests to the "direct relationship between the concentration of valuable metals in termite mounds and their contents in subsurface horizons of the regolith" **[35].** Using termite mounds as indicators for minerals is based on the "assumption that the mound-building process results in an upward transfer of clay, silt, sand and fine valuable metals particles to the surface horizon, a process opposite to leaching"**[36]**. This often results in the mobilization and dispersion of trace elements **[36].** In Africa, termitaria occur ubiquitously as preserved or "eroded relict mounds of various sizes and structures in a gently undulating terrain" **[37].**

Geologically, most African landscape is made up of "alluvial plains, colluvial plains, flood plains, pediments, erosional plains, rolling hills, escarpments, isolated hills and ridges"**[37]**. A termitarium was harvested from Sheda Science and Technology (SHETSCO), Abuja Nigeria for iron extractions (**Fig. 2.4**). The collapse of these termitaria results in what we called clay mineral. Most termitaria contain Silica, Alumina, iron and other minerals which are the composition of a clay mineral.

Figure 2.4: Iron ore deposit at Sheda Science and Technology Complex SHESTCO, Abuja-Nigeria.

Iron ores deposits are classified based on the quantity of iron present. Low-grade iron ore has iron (Fe) content $\leq 45\%$ **[38].** Some deposit contains $\geq 60\%$ iron (Fe) **[39]** content. These are usually classified as "high-grade iron ore deposit" **[39]**. All "high-grade iron ore deposits" **[39]** are strongly enriched in Fe with a lesser amount of $SiO_2, Al_2O_3, MgO \wedge CaO$ as compared to the low-grade iron formation due to the leaching of quartz, Fe-silicate, and carbonates during enrichment and possibly precipitation of secondary iron oxides and iron oxyhydroxides **[40].** High-grade iron ores are grouped into three based on their colouration, i.e. yellow, blue, and red in **Fig. 2.5**. Blue iron ore is prevalent and is made up of hematite and martite with an iron content of ($65.7 \pm 2.4 wt.\%$¿**.** Yellow ore indicates the presence of a large quantity of goethite. The red ore contains a large percentage of alumina ($1.9 wt.\% Al_2O_3$¿, Silica and hematite.

This clay-mineral is slightly enriched in light rare-earth elements and a relatively low amount of trace-element are also found **[40].**

(a) (b) (c)

Figure 2.5: The different colouration containing iron ore: (A) Primary blues iron-ore deposit-Hematite-Richer, (B) Red iron ore deposit-clay minerals and (C) Soft, goethite-rich yellow iron ore deposit **[40]**.

The world's largest iron reserves are found in rocks formed 1.8 billion years ago. It is believed that, during this era, the earth's oceans consist of plenty of dissolved iron with almost no oxygen component. The iron ore deposit became evident when the first organism capable of photosynthesis began releasing oxygen into the waters **[30, 37]**. The oxygen component immediately combined with the abundance of dissolved iron to form the various oxides of iron such as hematite (Fe_2O_3¿, magnetite (Fe_3O_4) and so on. Geological basin and processes indicate that iron ore is categorized into three stages of formation on the earth's crust **(Fig. 2.6).**

These include;

I. Direct sedimentation forming bedded sedimentary iron ore deposits.

II. Igneous activity forming segregation (intrusive iron ore deposit).

III. Enrichment due to surface and near-surface weathering.

I. Sedimentary Iron Ore Deposit/Banded iron formation (BIF)

This method of iron ore deposit formation is a result of mineral precipitation from solutions. These iron ore “formations were created when solutions of iron oxides and silica precipitated in alternating layers”**[41]**. These form an iron oxide in the forms of hematite and magnetite. The associated gangue silica forms chert and alumina. Iron and “silica were supplied by volcanic activity common during the Precambrian period” **[41]**. The deposits accumulated formed distinctive grey (iron oxides) and red bands, hence the name "banded iron". This type of iron deposits is also called banded iron formation (BIF) **[41]**. These deposits contain 55 to 65% iron **[32].** In some structures, iron is a form of carbonate (siderite with magnesium, magnesium and calcium with siderite) or silicates (greenolite, Minnesota and stilponomelane) and lead sulfide (pyrite). Chemically, this iron formula contains “alumina (Al), sodium (Na), It contains potassium (K) and other abundant elements” **[41]**.

Banded iron formations (BIFs) are metamorphosed sedimentary rocks made up of mainly lightly bedded iron minerals and silica (e.g., Quartz). BIFs are associated with sequences consisting of mafic volcanic rocks, shales and dolomites **[41].**

II. Igneous Activity Forming Segregation (Intrusive Iron Ore Deposit)

Igneous origin is formed as a result of molten magma erupted from the earth core containing enough iron content which finally undergoes cooling (i.e., magmatic segregation of iron-bearing minerals). It is associated with genetically related volcanic and subvolcanic rocks. Ignite iron ore deposits are primarily associated with moderately acidic volcanic rocks and occur primarily in volcanic eruptions or in and around contact

areas within and around plutons. It is divided into “continental volcanic intrusive iron ore and marine volcanic intrusive iron deposits” **[42].** The iron content is generally about 20%, but it can be as high as 60% (high-grade iron ore). Most of the iron ore minerals occur as ilmenite, magnetite, or hematite **[43].**

III. Enrichment due to surface and near-surface weathering.

These deposits were formed by “weathering and leaching of abundant iron ore and/or iron-containing poly-metal ores, which were deposited on the remaining slopes” **[31]**. This type is “shallow, mainly small and medium-sized spares” **[31]**. Concentrations on or near the surface due to the removal of less tolerant minerals. Such reserves were a major source of iron ore before the development of methods to benefit hard ore. When existing iron-rich minerals (such as siderite and glauconite) are chemically and physically weathered during soil formation, iron oxide is gradually concentrated to form iron-containing sediments. Iron content varies between 50-60% **[31].**

(a) (b) (c)

Figure 2.6: Geological basin and processes: (a) Sedimentary iron ore (band iron formation), (b) Igneous iron ore deposit, (c) Weathered rock iron ore (clay mineral).

IV. **Hydrothermal deposits**

The hydrothermal solution has various metals dissolved in them. This solution eventually forms ore and the gangue mineral in response to change in solution usually due to a decrease in temperature. Provide majority of the earth metals such as lead, zinc, molybdenum and gold. Amongst others are our industrial materials such as iron, copper, clay mineral and quartz. This deposit is present due to the wide range of geological activities associated with granitic intrusion, sedimentary basin and ocean floor. Proximal hydrothermal deposit or magmatic magnetic deposits contains magnetite-hematite bodies which have replaced non-ferrous rocks like the major–constituents **[44].** Illustrations of the various hydrothermal deposit are presented **(Fig. 2.7).**

Deposit is considered viable for iron extraction only if it contains up to 25% iron. All deposits were subsequently affected by late-stage weathering, forming hard duricrusts above some deposits and remobilizing Fe and Mn.

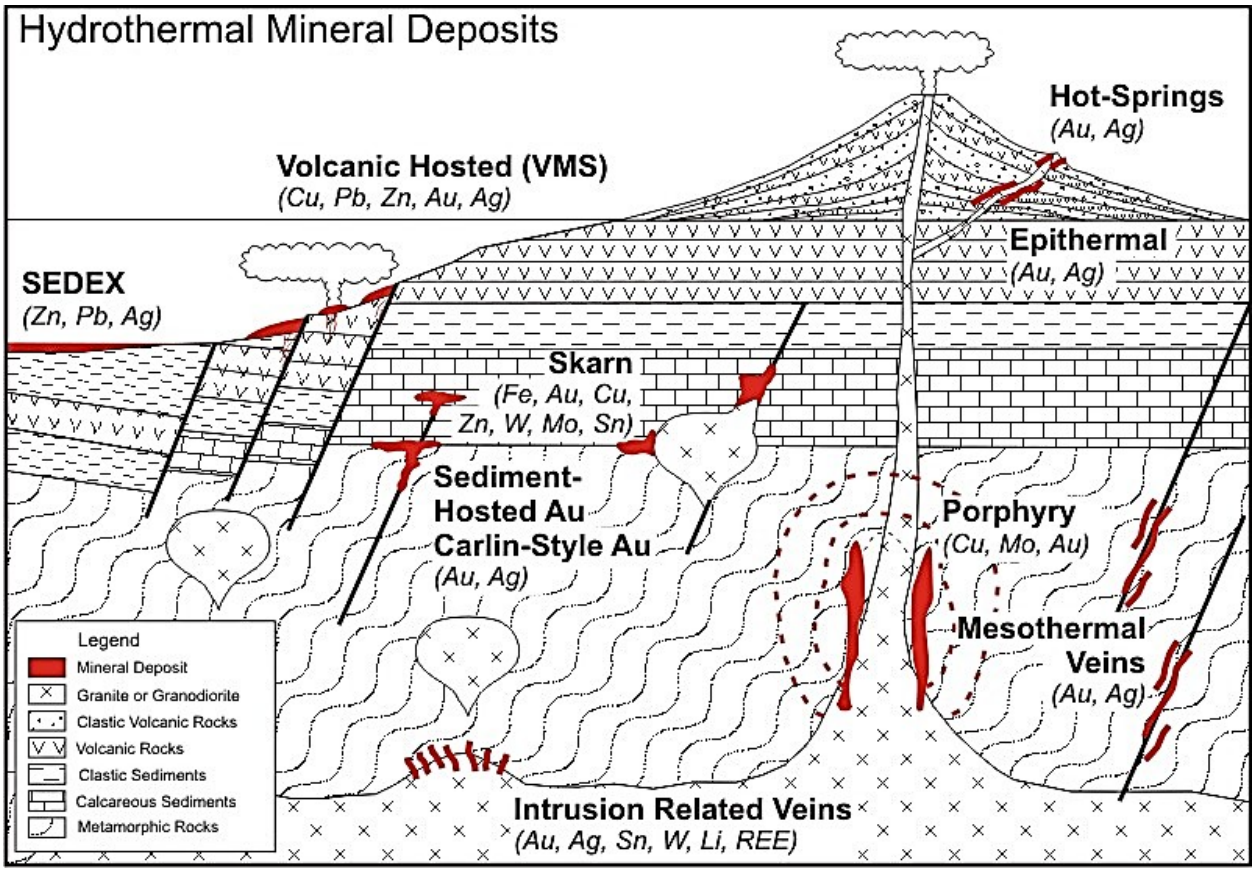

Figure 2.7: Illustrations of the various hydrothermal deposit **[45]**.

2.3 Types of iron Mineral

Several minerals contain iron, but minerals with high iron content for mining and beneficiation were considered. Over 300 minerals are found in iron ore, but only a few of them are considered relevant iron ore minerals. Below are some major iron minerals presented in **Table 2.1.**

Table 2.1: **Property of Major Iron Minerals [45]**.

Minerals	Chemical Formula	Theoretical iron content	Specific gravity	Mohs Hardness
Hematite	Fe_2O_3	70	5.1	5-6
Magnetite	Fe_3O_4	72	5.2	5.5-6
Martite	$\alpha - Fe_2O_3$	70	5.3	5.5-6.5
Goethite	FeO(OH)	63	3.3-4.3	5-5.5
Siderite	$FeCO_3$	48	4	4
Chamosite	$(Mg, Fe, Al)_6(Si, Al)_{14}(OH)_8$	45	3.1	3
Pyrite	FeS_2	47	4.9	6-6.5
Limonite	$FeO(OH).n(H_2O)$	63	3-4	5-5.5
Lepidocrocite	$\gamma - Fe_2O_3.H_2O$	60	4.1	5
Greenalite	$Fe_3Si_2O_5$¿	45	2.9	3
Ilmenite	$FeTiO_3$	37	4.7-4.76	5-6

Hematite is one of the most abundant iron minerals on the Earth's surface in the shallow crust. Iron oxide with the chemical composition of Fe_2O_3. It is a common “rock-forming mineral found in sedimentary rocks, metamorphic rocks” **[46]** and hematite minerals, containing up to 66% iron and can be supplied directly to steel blasting furnaces. Their formation is not fully from shallow seas about 1.8-2.6 billion years ago, during the Precambrian period **[46, 47].** Hematite is paramagnetic (slightly attracted to a magnet), it becomes magnetic when heated or attached to magnetic magnetite hence are beneficiated using a magnetic separator. During the geological survey, if a specimen is found to be magnetic but has reddish streaks then is likely to be a combination of magnetite and hematite **[48].**

Magnetite (Fe_3O_4) is one of the main oxides of iron. It is “ferrimagnetic (i.e. attracted to a magnet) and can also be magnetized to become a permanent magnet”**[47]**. It is the most magnetic amongst all the naturally occurring iron mineral. It has higher iron content than hematite ore but often occurs in a lower amount. That means it has to be

concentrated during beneficiation. However, the “ore’s magnetic properties help separate magnetite ore from the rock during processing” **[47]**. Magnetite contains both “iron (II) oxide (FeO) and iron (III) oxide (Fe_2O_3)” **[47].** High-grade magnetite ore normally contains more than 60% iron with some impurities such as silica, alumina and phosphorus.

Martite (Fe_2O_3) is secondary hematite formed by chemically replacing “magnetite produced under depth and pressure” **[48]**. Usually, the magnetite particles are displaced along the crystal plane from the outer edge to the centre **[48].**

Goethite and Limonite (FeO(OH)) are iron minerals formed by “oxidation of iron carbonate, hematite, martite and magnetite”**[19]**. There are fragments of goethite in the quartz, of which goethite has replaced hematite. Goethite, which replaces “hematite, does not contain manganese, while goethite, which replaces carbonate and martensite”, contains a large amount of Mn (by weight, the Mn content is as high as 27%) **[19].** These are hydrated iron oxides with an iron content of up to 60-63%, which can appear as the main mineral and are always formed relatively close to the surface due to the weathering of the bare ore.

Siderite ($FeCO_3$) is a valuable iron ore because it contains 48% iron and does not contain sulfur or phosphorus. It only accounts for a small part of the world's iron ore reserves.

2.4 Gangue mineral associated with iron ore

Fe minerals contain oxygen as a primary element, they exist as oxides. However, some minerals found their way into these ores. During beneficiation, these minerals are

considered as the gauge. The iron is concentrated to reduces the associated gauge. The presence of these minerals has both good and bad effect. The four components forming slag in iron ore include “acidic silica (SiO_2) and basic calcium oxide (CaO), magnesium oxide (MgO) and neutral alumina (Al_2O_3)” **[49]**. Most iron ore contains excess “SiO_2, and the coke powder used for fuel is mainly composed of this oxide, so an alkaline stream, such as limestone, must be added” **[49]**. Iron ore contains silica is usually removed as a slag during the smelting process.

At temperatures above 1300 ° C, silicon dioxide is reduced to silicon, forming alloys with iron. The main function of silicon is to promote the formation of gray iron. Gray iron is less brittle and easier to machine than white iron, so it is best suited for casting. Reduced shrinkage and pitting have been reported with fewer defective castings **[50].**

Alumina contains iron in the form of “clay and magnesium-aluminium carbonate hydroxide ($Mg_6Al_2CO_3$ $(OH)_{16}.4H_2O$)”**[51]**. The viscosity of the slag increases due to the presence of alumina. This will cause slag thickness and slow loading due to the slow process. The high alumina content also makes it difficult to remove the slag, which can cause the furnace to freeze. Increasing lime flow will reduce viscosity **[51].**

2.5 Production and Consumption of iron mineral globally

The world's iron ore reserves are estimated to be “over 800 billion tonnes of crude ore and over 230 billion tonnes of iron” **[52]**. The “annual world production of iron ore is about one billion tons” **[52]**. Although “iron ore is produced in about fifty countries, the 10 largest producing countries account for more than 80% of the world's total production” **[52]**. **Figure 2.8** present the iron ore production distribution of the world.

The statistics (**Fig. 2.9**) below is an indication of the iron consumption within the 2018 and 2020

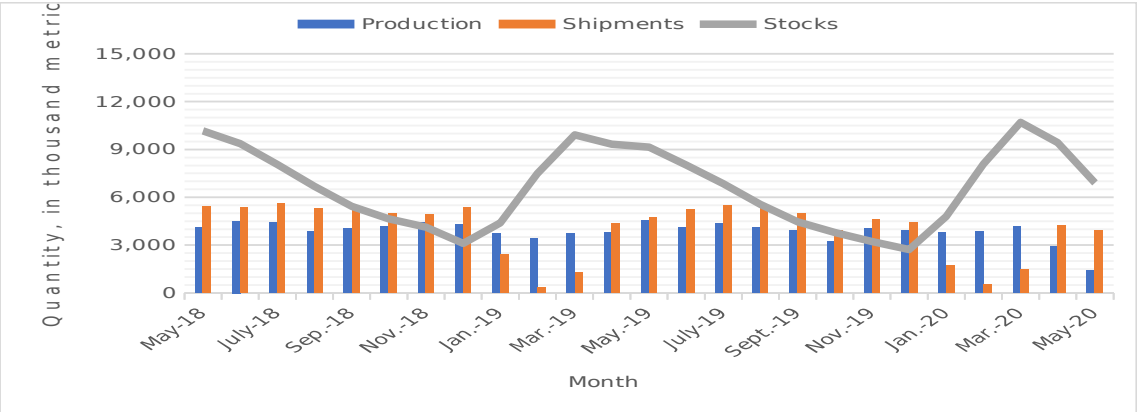

Figure 2.8: "Monthly domestic production, shipments, and stocks of iron ore from May 2018 through May 2020" **[14].**

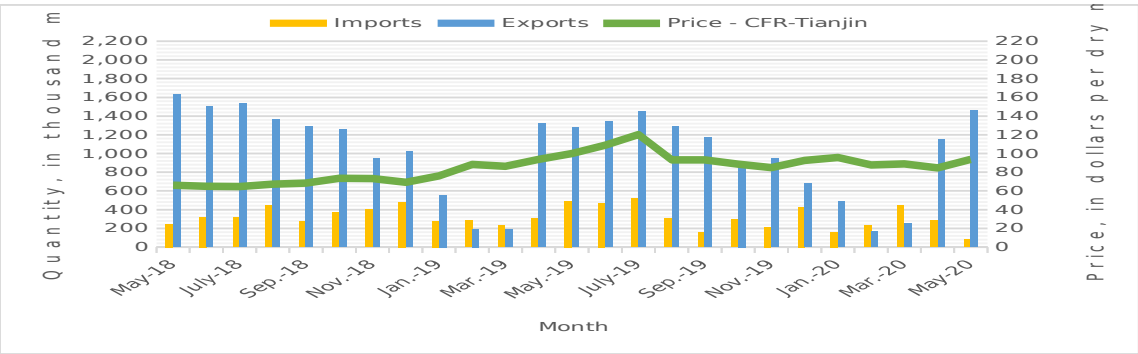

Figure 2.9: Monthly domestic import/export of iron ore and spot price of imported iron ore fine powder, 62% iron content, cost and transportation "(CFR) at Tianjin Port in China from May 2018 to May 2020. Source: US Census Bureau and Index Mandi" **[42].**

2.6 Iron Ore Mining

Iron ore can be mined by two main techniques. These are surface and underground methods. The decision to adopt underground or open-air mining techniques depends on the proximity to the surface of the ore body. Surface mining has to deal with the removal of the first overburden of the earth to expose the iron mineral for extraction.

In underground methods, the iron mineral is removed through shafts or tunnel. The clay mineral is extracted by surface mining. “Surface mining can be classified into two groups based on the method of extraction; mechanical extraction or aqueous extraction” **[32,51]**. “Mechanical extraction methods use mechanical processes in a dry environment to recover metals” **[32]**, including mining methods specified for Open-pit mining (i.e. “Opencast mining, Quarrying of dimension stone, Highwall/auger mining”).

The open and open method uses a conventional mining run-off to extract the minerals. Rock fracture usually occurs due to drilling and blasting of the reinforced material and drilling or removal directly with a drilling machine for loose soil and/or rock decomposition, and then handling and transporting the material.

Open-pit and opencast “mining accounts for about 96% of nonmetallic minerals, 87% of mineral ores and 60% of world coal production” **[51]**. Open-pit “mining is the most common mining method, producing nearly 85% of all minerals, excluding oil and natural gas” **[51]**. In open mines, iron ore production ranges from 0.5 to 30 million tons per year.

Bulk rock mining is very “similar to open-pit mining, but non-blasting rock crushing is used almost exclusively for cutting prismatic blocks or flat stone slabs”. The high labour intensity and the costs associated with cutting stone make excavation the most expensive open-pit mining method.

Liquid extraction generally “involves the use of water or a liquid solvent to remove minerals from subsurface sediments by hydraulic fracturing or physicochemical dissolution”.

Water extraction includes; Placer mining and Mining Solution

Placer mining is to obtain “heavy minerals from alluvial or placer deposits, using water to excavate, transport, and/or concentrate minerals” **[51]**. A mining solution is employed for “extracting soluble or fusible minerals using water or a lixiviant” **[32]**.

The underground method is used when the stress ratio of surface use at the depth of the straw (one or both) is very high. Underground iron ore is still mined in many large deposits in “some parts of the world, such as the Kirnwara mine in Sweden” **[32]** and “Kumba’s Thabazimbi Mine in South Africa” **[51].**

2.7 Iron ore processing

The processes of getting iron oxide from the ore involved several beneficiation and metallurgical techniques. The iron oxide content has to be concentrated to increase its amount in the residue. The hydrothermal process can be used to obtain high content “of iron oxide from a high-grade ore” **[30]**. With “low-grade ore” **[30]**, we need to beneficiate further to increase the concentration.

Generally, there are two techniques to beneficiating iron ore. These are either mechanical or Chemical process. The mechanical process involved hand-picking, dry/wet concentration, the use of a magnetic separator, electrostatic means, and froth floatation among others. Chemical methods include the use of chemicals to dissolve valuable minerals from Tailings. This advantage improves the physical and chemical properties of the iron oxide content **[30].**

2.8 Flowsheet of Iron Extraction

Processing routes for the extraction of iron ore is present in the illustration **(Fig. 2.10).** Size reduction is a key element in the beneficiation process of iron ore. “Crushing and grinding are used to increase the surface area of the iron ore from the mine”. Screening and classification help us to separate the particle size into various fraction based on the physical size, velocity in water and their specific gravity. The particle size has a contribution to the overall iron concentrate in the chemicals process.

Iron oxide has a huge application in several industries including biomedical. Each iron deposit has its mineralogy properties and specific mineral processing and metallurgical treatments are required to get the most out of it. The choice of mineral processing depends on the composition of the deposit, the gang, and the ore **[52].**

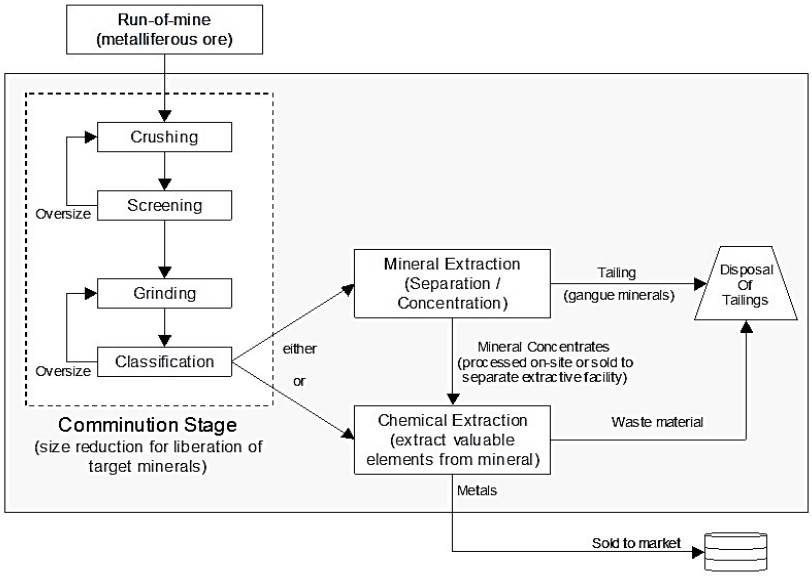

Figure 2.10: Flowsheet of the two processes of iron extraction **[52]**.

2.8.1 Crushing and Grinding

A lump of size range 2-1.25 m taken from the mine is reduced to a maximum size of 1-0.5 cm to liberate the iron oxides from the gangue, thus increasing its content. For some low-grade ore, a particle size of $45\,\mu m$ is recommended for a high-grade iron concentration was obtained. The first stage of grinding produces particles with a size of 5–6 cm. Factors to consider when determining the degree of ore crushing include iron concentrations in the ore, its minerality, hardness, and moisture content **[53].**

2.8.2 Concentration of Iron Oxide

The "concentration of valuable minerals from gangue involves the exploitation of the differences in the mineral properties of the ore after effective comminution" **[54]**. Mechanical or chemical methods are used to remove the iron from the gangue.

2.8.3 Hydrometallurgy

The use of chemicals to liberate iron oxide from its gangue is a way of increasing the iron concentrate. Controlling the temperature, particle size and acid concentration could enhance the iron reduction in the clay mineral. Several kinds of organic and inorganic acids **[54–62]** or "complexing reagents have been used in the dissolution of iron oxide" from clay minerals. These are the commonest reagent to "remove iron oxide and oxyhydroxides contain in clay mineral" **[63].** Most of this is focused on the "mechanism of dissolution of hematite and magnetite, testing different acid and experiment conditions" **[54, 55]**. Studies have been done using "oxalic acid for the dissolution of iron from kaolin clay" **[54–57].** A similar study was done using phosphoric

acid in iron removal from quartz **[64].** However, “goethite species have been removed with anionic surfactant increasing the whiteness index” of the gangue which indicate the dissolution of iron oxide **[61].** The use of phosphoric acid has greater leaching efficiency as compared to other leaching reagents.

Bioleaching is another technique for liberating iron oxide from clay mineral. It is an environmentally friendly method; “however, bacteria are usually very sensitive to the changes in the environment in which they occur”. It is important to “consider several factors such as atmosphere, temperature and pH that lead to more complex” processes. However, in this study, we used phosphoric acid solution for the chemical leaching process to reduce iron oxide from clay mineral.

2.9 Characterization Techniques

Different characterization methods are used to investigate the composition of clay mineral for the iron content and composition. The extend of hematite or magnetite, total iron content, and any of the impurities vary from source to source **[62].**

Eye studies using hand lenses and/or stereoscopic microscopes are performed macroscopically to collect information about elliptical deposits. Physical properties obtained from macroscopic studies include graphical or abstract properties of ores. Whether it is soft, hard and flaky, or a dust ore material.

Due to the limitation of the unaided eye, we need to investigate our sample using various methods. The microscopic studies identify the “major minerals present in the clay ore and the particle size of each component”.

2.9.1 Scanning Electron Microscopy (SEM)

High beam electrons are used to “probe the surface of a sample”. The “electrons interact with the atoms of the sample”, giving rise to the morphology, composition and surface topology as well as the electrical properties of the sample. Its high resolving power as compare to the light Microscopy.

2.9.2 Energy Dispersive Spectroscopy (EDS)

Energy dispersive spectroscopy (EDS) is an extension of SEM. It gives the percentage of elemental composition in the sample. EDS techniques are used to examine the elemental composition of our concentrate.

2.9.3 Fourier Transform Infrared Spectroscopy (FT-IR)

FT-IR techniques are used for determining the functional groups/chemical bonding in the sample. It is a non-destructive technique. “Chemical bonds vary widely in their sensitivity to probing by infrared techniques”. IR radiation penetrates the clay sample. Some radiations are absorbed by the sample and others pass (transmit) the sample. The “resulting spectrum represents the absorption” and permittivity of the molecule and forms the molecular fingerprints of the sample. Like a fingerprint. This “makes infrared spectroscopy useful for many types of analysis”.

2.9.4 UV/Vis Spectroscopy

UV-Vis spectroscopy is used to study iron absorption during the leaching process. In this process molecules in the sample absorbed visible wavelength (350 - 600 nm). This absorption gives a characteristic of the impurities present. In UV/Vis spectroscopy, when

monochromatic light passes transmit a solution of an absorbent, the rate of decrease in radiant intensity, which is proportional to the thickness of the absorbed solution, is proportional to the intensity. Incident radiation and solution concentration.

Given by **Equation (2.1):**

$$A = \log\left(\frac{I_o}{I}\right) = \varepsilon CL \qquad \textbf{(2.1)}$$

where **A** is the absorption, $\mathbf{I_o}$ is the intensity of the incident light on the sample cell, **I** is the intensity of light leaving the sample cell, **C** is the molar concentration of solute, and **L** is the optical path length (cm) of the sample cell. , and ε molar absorptivity coefficients.

Various nanoparticles have been synthesized for cancer detection and treatment due to their biocompatibility. Nano-sized materials have gained a lot of scientific focus in application to cancer treatment, target drug delivery, and so on **[64–66].** The beneficiation of iron oxide from clay mineral via chemical leaching is important for diverse applications. The focus of this work is on the characterization and synthesis of Iron oxide Particles via chemical leaching from bioinspired termite mound for biomedical application.

References

[1] A. Jemal, F. Bray, and J. Ferlay, “Global Cancer Statistics,” vol. 61, no. 2, pp. 69–90, 2011, DOI: 10.3322/caac.20107.

[2] L. A. Torre, F. Bray, R. L. Siegel, and J. Ferlay, “Global Cancer Statistics, 2012,” vol. 65, no. 2, pp. 87–108, 2015, DOI: 10.3322/caac.21262.

[3] D. M. Parkin, F. Bray, J. Ferlay, and A. Jemal, “Cancer in Africa 2012,” pp. 953–967, 2014, DOI: 10.1158/1055-9965.EPI-14-0281.

[4] GLOBOCAN 2020, "New Global cancer data," Cancer | WHO | Regional Office for Africa. 17 Dec 2020.

[5] F. Bray, J. Ferlay, and I. Soerjomataram, “Global Cancer Statistics 2018 : GLOBOCAN Estimates of Incidence and Mortality Worldwide for 36 Cancers in 185 Countries,” pp. 394–424, 2018, DOI: 10.3322/caac.21492.

[6] A. Jemal, F. Bray, D. Forman, M. O. Brien, and J. Ferlay, “Cancer Burden in Africa and Opportunities for Prevention,” 2012, DOI: 10.1002/cncr.27410.

[7] S. Nie, Y. Xing, G. J. Kim, and J. W. Simons, “Nanotechnology Applications in Cancer,” 2007, DOI: 10.1146/annurev.bioeng.9.060906.152025.

[8] W. R. Hanahan D, “The hallmarks of cancer.,” Cell 100, pp. 57–70, 2000.

[9] W. R. Hahn WC, “Modelling the molecular circuitry of cancer,” Nat. Rev. Cancer, pp. 2:331–41, 2002.

[10] L. L. Petricoin EF, Zoon KC, Kohn EC, Barrett JC, “Clinical proteomics: Discov., translating benchside promise into bedside reality,” Nat. Rev. Drug, pp. 1:683–95, 2002.

[11] P. E. Liotta L, “Molecular profiling of human cancer,” Nat. Rev. Genet., pp. 1:48–56, 2000.

[12] A. De Escosura-mun, C. Sa, M. M. Costa, and A. Merkoc, “Rapid Identification and Quantification of Tumor Cells Using an Electrocatalytic Method Based on Gold Nanoparticles,” vol. 81, no. 24, pp. 10268–10274, 2009.

[13] S. G., “Large clusters and colloids—metals in the embryonic stage,” Chem. Rev., pp. 92:1709–27, 2017.

[14] H. A., “Small-particle research—physicochemical properties of extremely small colloidal metal and semiconductor particles,” Chem. Rev, pp. 89:1861–73, 1989.

[15] A. P., “The use of nanocrystals in biological detection.,” Nat. Biotechnol., pp. 22:47–52, 2014.

[16] A. AP., “Semiconductor clusters, nanocrystals, and quantum dots.,” Science, pp. 271:933–37, 2001.

[17] L. C. Alivisatos AP, Gu WW, “Quantum dots as cellular probes,” Annu. Rev. Biomed. Eng., pp. 7:55–76, 2005.

[18] Pinaud F, Michalet X, Bentolila LA, Tsay JM, Doose S, et al. “Advances in

fluorescence imaging with quantum dot bio-probes," Biomaterials, pp. 27:1679–87, 2006.

[19] Michalet X, Pinaud FF, Bentolila LA, Tsay JM, Doose S., et al, "Quantum dots for live cells, in vivo imaging, and diagnostics.," Science (80), pp. 307:538–44, 2005.

[20] N. S. Gao XH, Yang LL, Petros JA, Marshal FF, Simons JW, "Vivo molecular and cellular imaging with quantum dots," I Curr. Opin. Biotechnol., pp. 16:63–72, 2005.

[21] N. S. Smith AM, Gao X, "Quantum dot nanocrystals for in vivo molecular and cellular imaging.," Photochem. Photobiol., pp. 80:377–85, 2014.

[22] N. S. Chan WCW, Maxwell DJ, Gao XH, Bailey RE, Han MY, "Luminescent quantum dots for multiplexed biological detection and imaging," Biotechnol., . Curr. Opin., pp. 13:40–46, 2002.

[23] Harisinghani MG, Barentsz J, Hahn PF, DesernoWM, Tabatabaei S., et al., "Prostate, Noninvasive detection of clinically occult lymph-node metastases in cancer.," Med., N. Engl. J., pp. 348:2491–99, 2003.

[24] Hood JD, Bednarski M, Frausto R, Guccione S, Reisfeld RA., et al. "Tumor regression by targeted gene delivery to the neovasculature. Science," pp. 296:2404–7, 2002.

[25] W. D. C. Biol., "Imaging optical sensor arrays," urr. Opin. Chem., pp. 6:689–95.

[26] Nicewarner-Pena SR, Freeman RG, Reiss BD, He L, Pena DJ, et al. "Submicrometer metallic barcodes.," Science (80-.)., pp. 294:137–41, 2001.

[27] Cunin F, Schmedake TA, Link JR, Li YY, Koh J., et al., "Biomolecular screening with encoded porous-silicon photonic crystals.," Nat. Mater., pp. 1:39–41, 2002.

[28] Dejneka MJ, Streltsov A, Pal S, Frutos AG, Powell CL., et al., "Rare earth-doped glass microbarcodes.," Proc. Natl. Acad. Sci. USA, pp. 100:389–93, 2003.

[29] M. C. Cao YWC, Jin RC, "Nanoparticles with Raman spectroscopic fingerprints for DNA and RNA detection.," Science (80-.)., pp. 297:1536–40, 2002.

[30] Wehleekema Siaplay, "Assessment of Iron Ore Mining Gangues in Itakpe," January 2017.

[31] B. Of. "Technical Resource Document, Extraction and Beneficiation of Ores and Minerals," in Office of Solid Waste, Special Waste Branch 401 M Street, SW Washington, DC 20460, pp. 530-R-94–030, 2016.

[32] P. Ferenczi, Iron ore, manganese and bauxite deposits of the Northern Territory. Northern Territory Geological Survey, Report 13, Government Printer of the Northern Territory Darwin, December 2001.

[33] D'Orey F.L.C., "Contribution of termite mounds to locating hidden copper deposits," Trans. Inst. Miner. Metall., vol. 84, pp. 150–156., 1975.

[34] E. Arhin and P. M. Nude, "Significance of regolith mapping and its implication for gold exploration in northern Ghana: A case study at Tinga and Kunche," Geochemistry Exploration. Environ. Anal., vol. 9, no. 1, pp. 63–69, Feb. 2009, DOI: 10.1144/1467-7873/08-189.

[35] R. Gleeson, C.F. & Poulin, "Gold exploration in Niger using soil and Termitaria.," J. Geochemical Exploration., vol. 31, pp. 253–283., 1989.

[36] Y. Roquin, C. Freyssinet, P.H. Novikoff A., and Tardy, "Geochemistry of termitaria and soils covering ferri-crete: Application to gold exploration in Western Africa.," in European Network on Tropical Laterite and Global Environment, Eurolat '91, Supergene Ore Deposits and Mineral Formation, 5th International Meeting, pp. 133–137, 1991.

[37] A. Petts, S. Hill, and L. Worrall, "Termite species variations and their importance for termitaria biogeochemistry: towards a robust media approach for mineral exploration." Geological Society Publishing House, 2009.

[38] G. A. Gross, "Geology of Iron Deposits of Canada," Iron Ranges Labrador Geosyncline. Geol. Surv. Canada, Econ. Geol. Rep. 22, vol. 3, p. 179., 1968.

[39] I. S. Stubbins, J.B., Blais, R.A. and Zajac, "Origin of the soft iron ores of the Knob Lake Range.," Can. Min. Metall. Bull., vol. Volume 585, pp. 43-58., 1961.

[40] J. Conliffe, "Geology and Geochemistry of High-Grade Iron-Ore Deposits in the Kivivic, Timmins and Ruth Lake Areas, Western Labrador," Curr. Res., pp. 1–26, 2016.

[41] S. Syed, "A green technology for recovery of gold from non-metallic secondary sources," Hydrometallurgy, vol. 82, no. 1–2, pp. 48–53, Jul. 2006, DOI: 10.1016/j.hydromet.2006.01.004.

[42] S. Adiloğlu et al., "We are IntechOpen, the world ' s leading publisher of Open Access books Built by scientists, for scientists TOP 1 %," Intech, vol. i, p. 13, 2012. DOI: 10.1016/j.colsurfa.2011.12.014.

[43] H. L. "Hydrothermal alteration, in Barnes, Geochemistry of hydrothermal ore deposits (2d ed.) | AZGS." https://www.azgs.arizona.edu/azgeobib/hydrothermal-alteration-barnes-hl-ed-geochemistry-hydrothermal-ore-deposits-2d-ed (accessed

Oct. 29, 2020).

[44] A. Australian Mineral Foundation, “Evidence of a magmatic fluid and metal source for Fe-oxide Cu- Au mineralisation: In Porter TM Hydrothermal iron-oxide copper-gold and related ore deposits: a global prospective,” Pollard, P., pp. 27–41, 2000.

[45] S. Timbillah, P. N. Aabulleh, and E. A. Agorhom, “Iron ore surge in the world - The role of Ghana,” Australas. Inst. Min. Metall. Publ. Ser., no. November, pp. 197–202, 2007.

[46] CharlesAmikiya, “Characterisation Of Iron Ore-A Case Study Of Mount Tokadeh, Western Nimba Area, Liberia By Charles Ayingayure Amikiya, BSc. Chemistry (Hons),” 2014.

[47] D. A. Brobst and W. P. Pratt, “United States Mineral Resources,” 1973. DOI: 10.3133/PP820.

[48] “Applied Mineralogy in the Mining Industry - 1st Edition.” https://www.elsevier.com/books/applied-mineralogy-in-the-mining-industry/petruk/978-0-444-50077-9?aaref=https%3A%2F%2Fwww.google.com%2F (accessed Oct. 29, 2020).

[49] “Principles of Extractive Metallurgy (Mcgraw Hill Series In Materials Science And Engineering): Rosenqvist, Terkel: 9780070539105: Amazon.com: Books.” https://www.amazon.com/principles-extractive-metallurgy-materials-engineering/dp/0070539103 (accessed Oct. 29, 2020).

[50] U. S. G. Survey, “Mineral Commodity Summaries 2011,” DOI: 10.3133/mineral, 2011.

[51] T. A. Le, “SME Mining Engineering Handbook 2nd Edition Volume 2 and Chemicals Brown & Root Braun.” Accessed: Oct. 29, 2020. [Online]. Available: https://www.academia.edu/6332369/SME_Mining_Engineering_Handbook_2nd_Edition_Volume_2_and_Chemicals_Brown_and_Root_Braun.

[52] P. Maddali, “Mineral Processing Technology (Mpt-2005) Tata McGraw-Hill Publishing Company Limited New Delhi.” Accessed: Oct. 29, 2020.

[53] M. J. Lee, S.O.; Tran, T, Jung, B.H.; Kim, S.J.; Kim, “Dissolution of iron oxide using oxalic acid. Hydrometallurgy,” vol. 87, pp. 91–99, 2001.

[54] F. R. . Martínez-Luévanos, A.; Rodriguez-Delgado, M.G.; Uribe-Salas, A.; Carrillo-Pedroza and J. G. Osuna-Alarcón, “Leaching kinetics of iron from low grade kaolin by oxalic acid solutions. Appl. Clay Sci.,” vol. 51, pp. 473–477, 2016.

[55] A. M. Veglio, F.; Passariello, B.; Toro, L.; Marabini, “Development of a bleaching process for kaolin of industrial interest by oxalic, ascorbic, and sulfuric acids: Preliminary study using statistical methods of Res., experimental design. Ind. Eng. Chem.,” vol. 35, pp. 1680–1687., 1996.

[56] F. K. Legorreta García, “study of iron leaching from Kaolinitic clay using oxalic acid European.,” Eur. Sci. J., pp. 11, 21–22, 2011.

[57] A. Panias, D.; Taxiarchou, M.; Paspaliaris, I.; Kontopoulos, “Mechanisms of dissolution of iron oxides in aqueous oxalic acid solutions. Hydrometallurgy,” vol. 42, pp. 257–265, 2005.

[58] L. E. . J. Hernández, H.; García, F.L.; Hernández Cruz, “Kaolin bleaching by leaching using phosphoric acid solutions.,” A.B. J. Mex. Chem. Soc., vol. 59, pp. 198–201, 2016.

[59] T. I. Zhang, Z.; Li, J.; Li, X.; Huang, H.; Zhou, L.; Xiong, “High-efficiency iron removal from quartz sand using phosphoric acid.,” J. Miner. Process., vol. 114, pp. 30–34, 2017.

[60] F. J. M. Legorreta García, “Statistical treatment of bleaching kaolin by iron removal.,” Chem. Soc., vol. 57, pp. 261–266, 2016.

[61] M. Ambikadevi, V.R.; Lalithambika, “Effect of organic acids on ferric iron removal from iron-stained kaolinite.,” Appl. Clay Sci., vol. 16, pp. 133–145, 2015.

[62] M. L. Aguilera, N.H.; Jackson, “Iron oxide removal from soils and clays.,” Soil Sci. Soc. Am. J., vol. 17, p. 359, 2018.

[63] B. Lavina, P. Dera, and R. T. Downs, “Modern X-ray Diffraction Methods in Mineralogy and Geosciences,” Rev. Mineral. Geochemistry, vol. 78, pp. 1–31, 2014, DOI: 10.2138/rmg.2014.78.1.

[64] R. H. W. Lee Eun-Young, Cho Kyung-Suk., “‘Microbial Refinement of Kaolin by iron-reducing bacteria’.,” Appl. Clay Sci. pp., vol. Vol. 22, pp. 47-53., 2002.

[65] K.-S. C. Eun-You L., “‘Microbial removal of Fe (III) impurities from clay using Reducers’, dissimilatory iron,” Biosci. Bioeng., vol. Vol. 87, pp. 397-399., 1999.

[66] T. L. Veglio F., “‘Process development of kaolin pressure bleaching using carbohydrates in acid media’.,” Miner. Process., vol. Vol. 41, pp. 239-255., 1994.

CHAPTER THREE

3.0 MATERIALS AND METHODS

3.1 Materials

Clay ore was used as the primary material for recovering iron oxide which was manually dug out from an earth-based termite mould (Fig. 3.1) at Sheda Science and Technology Complex (SHETSCO), Abuja-Nigeria. Diluted phosphoric acid (H_3PO_4¿ solution was procured from Guangdong Guanghua Sci-Tech Co. Ltd (Shantou, Guangdong, China) which served as the chemical used for leaching iron from the clay ore. Laboratory mortar and pestle, and a set of four sieves were used. Experiments were conducted at the African Development Bank (ADB) Multipurpose Laboratory “at the African University of Science and Technology, Abuja, Nigeria”. Phosphoric acid, sodium hydroxide, sulphuric acid (analytical grade), cotton wool, and syringes were obtained from the Biomaterials Lab of the ADB Multipurpose Lab at the African University of Science and Technology in Abuja-Nigeria.

(a) (b)

Figure 3.1: Sample Collection: (a) Termitarium Mould and (b) Dug Out Sample.

3.2 Experimental Procedures

3.2.1 Chemical Leaching of Iron

Comminution and particle size reductions were carried out in the laboratory using a mortar and pestle. Particle size analysis was performed using four sieves stacked in a vertical direction **(Fig. 3.2)** to obtain $45\mu m$ as recommended **[1]**. These processes were intended to increase the concentration of iron context in the ore and consequently enhance the leaching process.

(a) (b) (c) (d)

Figure 3.11: Comminution Process and Particles Size Analysis of Clay Ore: (a) Dug Out Sample Clay Ore, (b) Grinding Process with a Laboratory Mortar and Pestle, and (c) Sieving Process, (d) Sieved Particles to $45\,\mu m$.

Leaching experiments were carried out in a beaker as illustrated (**Fig. 3.3a-b).** Heating was done with a magnetic stirring/heating mantle (set at a constant temperature of 100℃¿. The "temperature was regulated with a thermo-regulator as incorporated in the equipment" **[2].** All "leaching tests were done at atmospheric pressure for 2 hours" **[1]**. For each set of experiment, 500 mL of phosphoric acid was used. The concentration of the phosphoric acid used in the leaching processes was as follows; "0.1 M, 0.5 M, 1.0 M, and 3.0 M as guided by a previous study" **[1]**, while the temperature was kept constant at 373.15 K (100℃) **[2].** This was intended to determine the effects of acid concentration on the removal of iron from the clay ore.

Sodium hydroxide and Sulphuric Acid was used to ensure experiments were kept constant at a pH of 1.0. **[1, 3]** using a pH meter as a measuring tool. The 1.0 M and 3.0 M solution has pH less than 1, hence little drops of dilute Sodium hydroxide were added to adjust the pH to1. Sulphuric acid (H_2SO_4) was used to adjust the pH of the 0.1 M and 0.5 M since they have pH greater than 1. Then, 25.0 g of clay samples were determined using an analytical weighing balance (Ohaus DV-114C Discovery, $110\,g \times 0.1\,mg$ Parsippany, NJ, USA). The measured sample was added to the flask under constant stirring at 700 revolutions per minute (rpm). Periodically, a sample of 12 mL was taken with a pipette from the leach slurry at 30 minutes interval and stored in 15 ml falcon tubes as shown (**Fig. 3.3c**). Samples were further filtered and centrifuged at 5000 rpm for 10 min. 12 mL slurry was taken from the solution **(Fig. 3.3d)** for the iron oxide determination as guided **[2]** using an ultraviolet-visible spectroscopy analysis (UV-vis spectroscopy).

(a) (b) (c) (d)

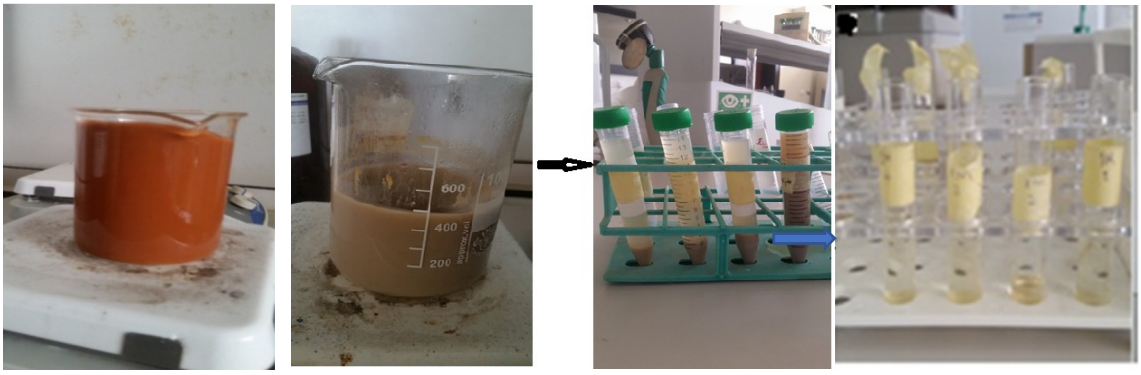

Figure 3.3: Leaching Process and Iron Determination: (a) initial heating and stirred with a magnetic stirrer at 100℃, (b) final state of leaching, **(c)** A 12 ml of slurry taken at 30 minutes interval, and (d) centrifuged aliquot for total iron determination.

The reaction of phosphoric acid with the clay ore sample as shown in **Figure 3.3a** indicates the initial stages of a reaction in progress. At a constant temperature under continuous stirring, the final leached process is arrived at in **(Fig. 3.3b).** 12 mL of the slurry was collected at 30 minutes interval for further analysis (**Fig. 3.3c).** In **Figure 3.3d,** the slurry was filtered and centrifuged to produce a clear homogenous solution for UV/Vis examination. The residue from the leached sample is filtered and dried in an oven at 160℃, while studies were conducted to compare with the unleached clay sample.

3.2.2 Sample Characterizations

The clay samples were analyzed with different characterization techniques including, morphological and elemental analysis using a scanning electron microscope (SEM) with EDS) (Evo LS 10, Carl Zeiss, Berlin, Germany) , functional group determination using Fourier transform infrared (FTIR) spectrophotometer and the absorbance of iron in a solution using an ultra-violet visible (UV-Vis) spectroscopy.

3.2.2.1 Morphological Characterization

Morphological analysis on both raw and leached sample “was investigated using a scanning electron microscope (SEM) (Hitachi S-3400N, Berlin, Germany)” at a magnification of 693 ×. The powdered sample was placed gently on a stub glued directly to a carbon tape followed by using a blower to blow out excess dust to avoid the dust from getting into the SEM machine. The samples were then coated with gold to enhance image visibility. A current at 10 mA was supplied for 45 seconds. The SEM machine was then stopped and vented. SEM vacuum was pumped for about 13 mins. The entire morphology of the sample was viewed under the SEM. An EDS session was carried out to investigate the elemental composition of the clay ore.

3.2.2.2 Fourier Transform Infrared Radiation Spectroscopy Analysis

Analysis of the functional group was determined with FTIR. Spectra of transmission versus wavenumber were plotted from 500 nm to 4000 nm.

Samples were pelletized for the FTIR analysis. Potassium bromide (KBr) salt was mixed with the samples (raw and leached samples) homogeneously, while a spacer (Ofite, Houston Texas, USA) was used to form pellets of the samples. The mixture was prepared into pellet using a portable hydraulic press for 5-10 min. The palletizer (Ofite, Houston Texas, USA) was used to compact the samples at 11,000 Psi. The pellet formed was analyzed with a Thermo-Scientific Nicolet iS5 FTIR machine (Berlin, Germany) making sure the sample is light enough to allow the passage of light.

3.2.2.2 UV/Vis Spectroscopy

The optical absorbance of iron leached was analysed with a “UV/Vis spectrophotometer (Specord 200-plus, Analytik Jena, Berlin, Germany)” **(Fig 3.4).** Phosphoric acid was used as a blank. The aliquot is a solution of phosphoric acid and iron oxide. Clean cotton wool was used to wipe the transparent region of the cuvette to avoid having fingerprints which can alter the result. After gently placing the sample in the UV-vis machine, the system was initialized and measurements were taken.

The UV-Visible absorption spectrum is the preliminary characterization used to determine the optical property of iron oxide in solution. The “narrow absorption spectrum at 412 nm was observed in UV-Vis spectra for nanoscale iron particles”. The bandgap energy of synthesized particles was given by:

$$E = hc/\lambda \qquad (3.1)$$

“where h is the Plank's constant, c is the velocity of light, and λ is the wavelength. The bandgap value of iron oxide was found to be 4.825 eV” **[11].**

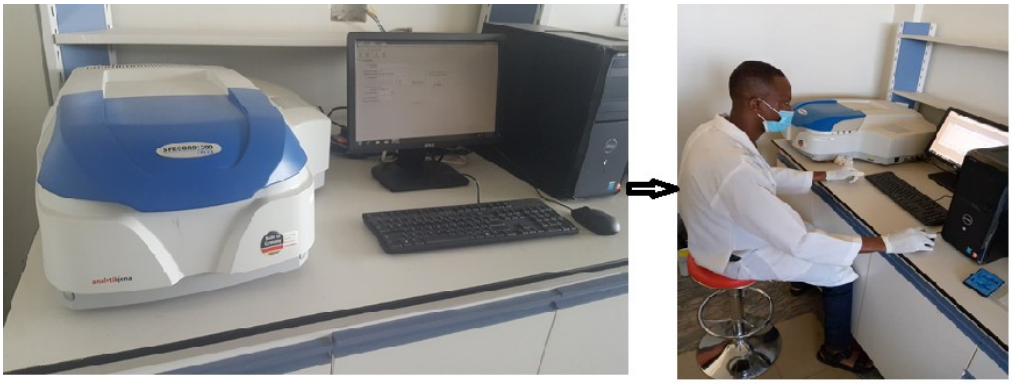

Figure 3.4: Determination of the absorption of iron oxide nanoparticles using a UV-Vis.
The absorbance and concentration of iron leached were characterized using Beer-Lambert Law which follows **[6]:**

$$C = \frac{A}{L\varepsilon} \quad \textbf{(}3.2\textbf{)}$$

"where A is the absorbance of iron in solution, ε is the molar absorptivity, C is the concentration of iron eluted, L is the path length of the cuvert or interaction distance of light as it travels through the sample (1cm)". The kinetics of leaching was then studied further studied and reported.

3.3 Leaching Kinetics

The Kinetic and order of reactions were studied. The leaching of iron oxide is influenced by the concentration of the phosphoric acid solution maintained at a temperature of $100\,℃$. The results were analysed with the "shrinking core model for heterogenous reaction under both diffusive and chemical control". "Leaching of iron oxide from clay sample can be explained with the shrinking core model" **[3,6]**:

$$a\,A_{Fluid} + b\,B_{particles} \rightarrow product \quad \textbf{(}3.3\textbf{)}$$

In the diffusion regime, the "reaction rate was controlled through the inert product layer". Therefore, the integrated reaction equation is given by:

$$1 - \frac{2}{3}X - (1-X)^{\frac{2}{3}} = K_d t \quad \textbf{(}3.4\textbf{)}$$

where **X** is the fraction reacted, $\mathbf{k_d}$ is the rate constant, and **t** is the reaction time. If the reaction is controlled by a chemical, then Equation **(3.4)** would be transformed into **(3.5)**

$$1 - (1-X)^{\frac{1}{3}} = k_c t \quad \textbf{(}3.5\textbf{)}$$

"where X is the fraction reacted, **t** is the reaction time, and k_c is the rate constant"

3.4 Kinetics Models of Iron Release Rates

The kinetics of iron release was investigated using kinetics models as presented in Table 3.1. The rate laws are used to determine the reaction path of the experiment. The zero-order kinetics model defines the process of Fe release from the clay mineral, but independent of the acid concentration. Hence to examined the zeroth-order kinetics, from the leaching experiments, a graph of accumulated iron concentration in solution was plotted against time. A linear plot relation between iron concentration as a function of time will be determined via the regression coefficient (R^2). The value of R^2 predicts the goodness of fit.

Also, first-order kinetics release was investigated by plotting the log of "iron concentration in solution as a function of time" (i.e., log % of Fe concentration vs. time). This model was evaluated graphically by comparing the value of R^2 with other models for the goodness of fit. The second-order model was also investigated in a similar manner, however, the search for a linear graph between the inverse of iron concentration versus time was used.

The **Higuchi model** includes both dissolution and diffusion. Some mathematical models explain the dissolution and/or release of iron Fe from clay minerals. As evidence of the adoption of iron leaching studies, the Higuchi equation itself has become a major equation of motion and is recognized as an "important factor in the development of drug delivery" in modern times of sustained release. The data obtained were plotted as the square root of cumulative Fe emissions vs. total time **[7].**

Therefore, the simple Higuchi model will result in a linear Fe concentration versus $\mathbf{t^{1/2}}$ plot with a slope, equal to $\mathbf{K_H}$ **[7].** Again the value of the $\mathbf{R^2}$ on data analysed is compared with other models. Therefore, if the correlation coefficient in the plot is high, it can be assumed that the main mechanism of **Fe** release is the diffusion-controlled release mechanism.

Table 3.1: Linear Relations of the Model Equations **[7].**

Model	Equation
Zero-order	$C_{Fe(t)} = C_{Fe(t_o)} + k_o t$
First-order	$\ln C_{Fe(t)} = \ln C_{Fe(t¿¿o)} + k_1 t¿$
Second-order	$\frac{1}{C_{Fe(t)}} = \frac{1}{C_{Fe(t_o)}} + k_2 t$
Higuchi	$C_{Fe(t)} = k_H t^{\frac{1}{2}}$

where $\mathbf{C_{Fe}}$ is the iron concentration at the time**, t,** $C_{Fe(t_o)}$ is the concentration at t = 0, **k** is the rate constant for the given model, k_H is the Higuchi constant, **C** is the concentration of the reactant species, t is the reaction time. The unit of the rate constant for each of the order of reactions is given as k_0 (L/mol. min^{-1}), k_1 (min^{-1}) and k_2 (L/mol. $min)^{-1}$, k_H (L/mol. min^{-1}), represent the apparent kinetic rate constants of zeroth, first, second-order reaction kinetics, and Higuchi model, respectively. The order of reaction, as well as the

kinetics behaviour for each of the experiment, were determined using the linear relationships from the equations presented in **Table 3.1** above.

References

[1] U. P. Acid, "Kinetics of Iron Leaching from Kaolinitic Clay, Using Phosphoric Acid," 2016, DOI: 10.3390/min6030060.

[2] A. Martínez-Luévanos, M. G. Rodríguez-Delgado, A. Uribe-Salas, F. R. Carrillo-Pedroza, and J. G. Osuna-Alarcón, "Leaching kinetics of iron from low grade kaolin by oxalic acid solutions," *Appl. Clay Sci.*, vol. 51, no. 4, pp. 473-477, 2011, DOI: 10.1016/j.clay.2011.01.011.

[3] S. I. Patterson, S.H.; Murray, H.H.; Lefond, "Industrial Minerals and Rocks;," AIME New York, NY, USA, 1983.

[4] K. Orisekeh *et al.*, "Processing of α -Fe_2O_3 Nanoparticles on Activated Carbon Cloth as Binder-Free Electrode Material for Supercapacitor Energy Storage," *J. Energy Storage*, no p. 102042, 2020. DOI: 10.1016/j.est.2020.102042.

[5] G. Jagathesan and P. Rajiv, "Biocatalysis and Agricultural Biotechnology Biosynthesis and characterization of iron oxide nanoparticles using Eichhornia crassipes leaf extract and assessing their antibacterial activity," *Biocatal. Agric. Biotechnol.*, Vol. 13. 2017, pp. 90-94, 2018. DOI: 10.1016/j.bcab.2017.11.014.

[6] J. D. L. and D. F. S. S. K. Kohl, "Demonstration of Absorbance Using Digital Color Image Analysis and Colored Solutions.," *Chem. Educ.*, vol. 83 (4), pp. 644-646, 2016.

[7] H. K. Shaikh, R.V. Kshirsagar, S.G. Patil. Mathematical models for drug release characterization: A review. World Journal of pharmacy and pharmaceutical sciences. Vol. 4(4) (2015) 324-338, 2017.

CHAPTER FOUR

4.0 RESULTS AND DISCUSSION

4.1 Material Characterization

4.1.1 Morphological Analysis

The Scanning Electron Micrograph, SEM for the raw sample is presented in Figure 4.1 below. **Figure 4.1(a)** is the SEM image of the raw sample. It was observed with irregular alumina particles with silica and small interfacial iron oxide particles. **Fig 4.1(b)** shows the particle size distribution from the SEM image. Particles with a diameter between 10-20 μm were the dominant particle size observed with the higher count. Smaller particles were also observed to be between 0-10 μm. Smaller particle is recognized with larger surface areas to chemical leaching, hence the need for comminution process in the first place.

(a) (b)

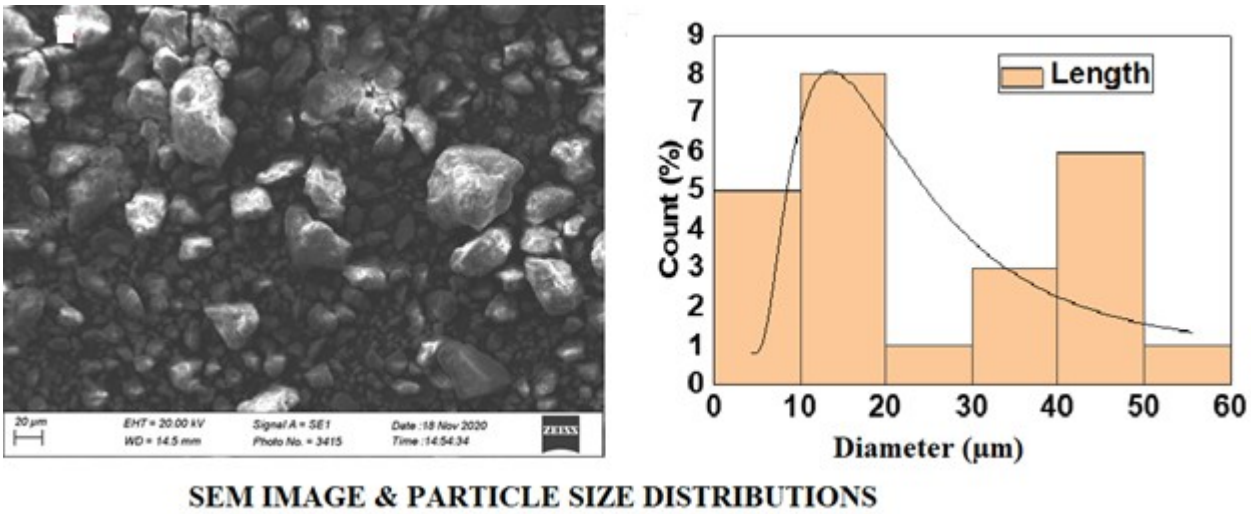

SEM IMAGE & PARTICLE SIZE DISTRIBUTIONS

Figure 4.1: Particle Size Analysis of Raw Clay Sample: (a) Scanning Electron Micrograph of and (b) the Particle Size Distributions.

4.1.2 Elemental Analysis

Elemental analysis was done with EDS (Evo LS 10, Carl Zeiss, Berlin, Germany) on them as sourced clay ore. The selected area marked in **Fig. 4.2 (b)** gave Al, Si, Fe and Au. These elements are expected considering that we are dealing with a clay sample. The main composition of clay is alumina and silicon. The iron oxide is detected because of the geological activities of the termites. The presence of gold (Au) was from the sputter coating done on samples before EDS analysis. The results thus indicate the presence of major oxides such as (SiO_2), AlO_3, Fe_2O_3, and other elements in a small amount. **Table 4.1** present the amount of each element present in the sample. The raw sample is made up of 16.92% iron with other associated elements. The percentage of iron found indicates that we have low-grade iron ore.

(a) (b)

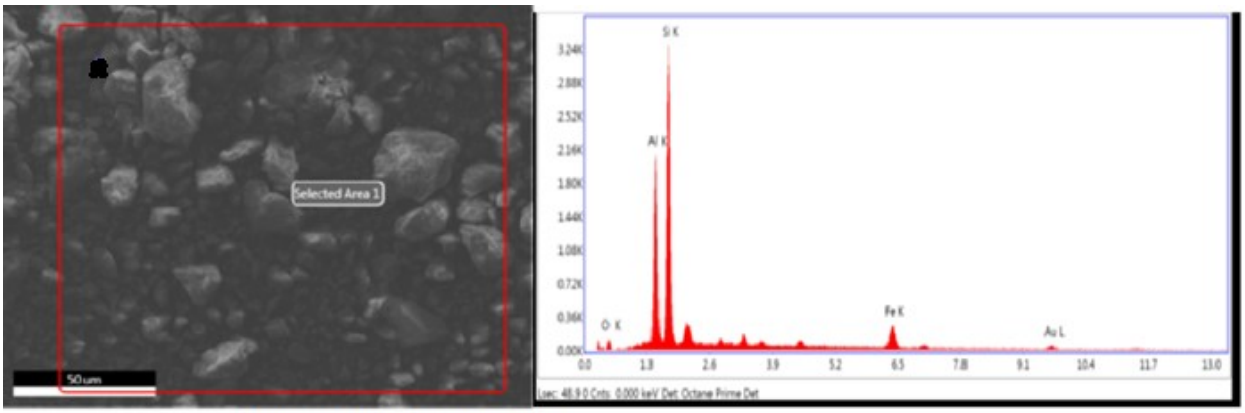

Figure 4.2 Elemental Analysis with EDS on Raw Sample: (a) Optical Image and (b) Elemental Compositions.

Table 4.1: Electron Dispersive Spectroscopy, EDS Compositional Analysis.

Element %	Weight %	Atomic %	Error	Net Int.	K Ratio	Z	R	A	F
O K	0.00	0.00	0.00	99.99	0.000	1.194	0.894	0.239	1.00
Al K	20.96	27.94	242.66	5.60	0.157	1.071	0.942	0.692	1.008
Si K	45.38	58.11	466.20	5.79	0.311	1.096	0.951	0.624	1.003
Fe K	16.92	10.90	66.03	6.21	0.166	0.934	1.025	0.969	1.084
Au K	16.73	3.06	9.75	36.13	0.125	0.634	1.120	1.027	1.149

4.1.3 Fourier Transform Infrared Radiation Spectroscopy Analysis

The absorbance of iron in the raw sample as a function of wavenumber was determined with FT-IR (Nicolet iS5, Thermo-scientific, Berlin, Germany). FTIR "analysis was conducted to identify the functional groups" and nature of bonds formed in the range of 500-4000 cm^{-1} **(Fig. 4.3a-c)**. **Figure 4.3** presents the combined effect of spectra alignment of raw and leached clay sample. The FTIR spectrum (**Fig. 4.3a)**

contains a peak at 462.8 cm^{-1} indicating the presence of quartz due to SiOH and SiO_2 **[9, 10].** The peaks around 897.47 cm^{-1} and 1026.70 cm^{-1} indications of the presence of kaolinite by the O-H bending band of Fe-OH. A peak of 1026 cm^{-1} indicates the possibility of C-O-C asymmetric stretch. The presence of H–O–H bends in water was found at 1226 and 2552 cm^{-1} **[32].** The C-H bond is present at the peak of 3005 cm^{-1} with a 3447.7 cm^{-1} O-H bond, the expansion and contraction vibrations. This indicates the presence of O-H and H–H peaks at 3526 and 3626.4 cm^{-1} stretchings **[9]**. A peak which is found around 3690.3 cm^{-1} indicates the presence of kaolinite. The resulting spectrum represents the absorption and transmission and forms the molecular fingerprints of the sample. Like fingerprints, the two unique molecular structures do not produce the same infrared spectrum. This makes infrared spectroscopy useful for many types of analysis.

In **Fig. 4.3 (b)** there is a peak shift from 1026 to 1045 cm^{-1} indicating a structural change due to iron removal. This is reflected in the UV/Vis data presented.

(a)

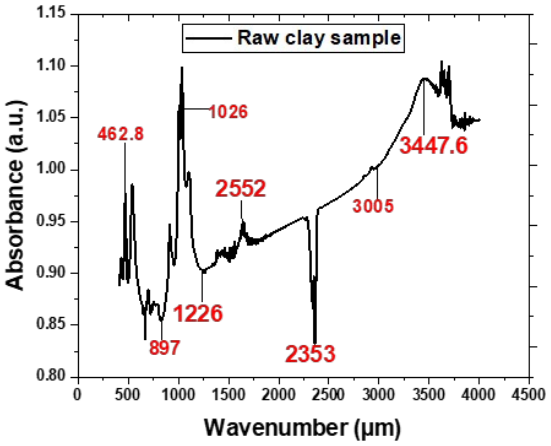

(b)

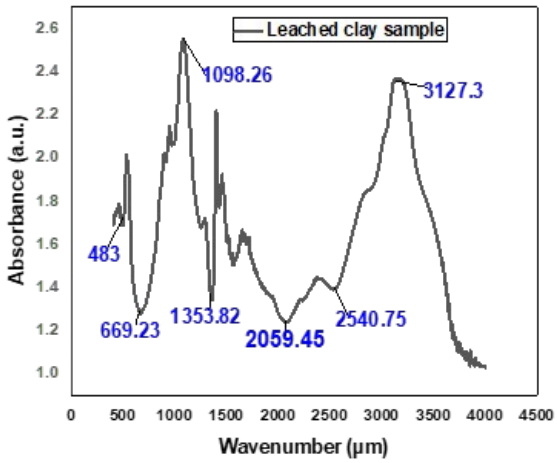

(c)

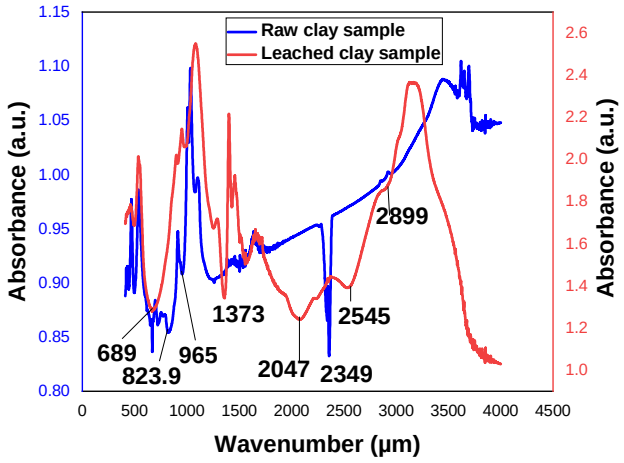

Figure 4.3: FTIR Spectra of (a) the as Sourced Sample Clay, (b) Leached Clay sample, and (c) combined Absorption Spectra.

4.2 Release Kinetics of Iron From Termite Mound

The UV-Visible absorption spectrum is the preliminary characterization used to determine the optical property of iron oxide in solution. UV/Vis results are presented in **Figure 4.4a-d**. Absorbance peaks of iron oxide were observed within the range of 350 to 600 nm for each of the acid concentrations. A narrow absorption spectrum at 408 nm, 410 nm, 412 nm and 414 nm was observed on the UV-Vis spectra for 0.1 M, 0.5 M, 1.0 M and 3.0 M phosphoric acid solution concentrations respectively. Similarly, the concentration of iron oxide was also determined. The filtrate iron oxide under UV/Vis spectroscopy gives a distinct hematite colloids absorbance at 412 *nm* which agreed with the literature **[1, 2].** The results epitomized our main objective of synthesizing iron oxide from Earth-based termite mould.

Following the leaching process with the phosphoric acid solution, the amount of iron released into the solution was characterized by a UV-Vis spectrophotometer (Specord 250 Plus, Analytik Jena, Berlin, Germany). From the Beer-Lambert law presented in the methodology section, the absorbance peak of iron oxide in solution was observed within the range of $350-600\,nm$ (**Fig. 4.4).** Moreover, iron concentration versus absorbance is presented in the standard curve below **(Fig. 4.5a-d).**

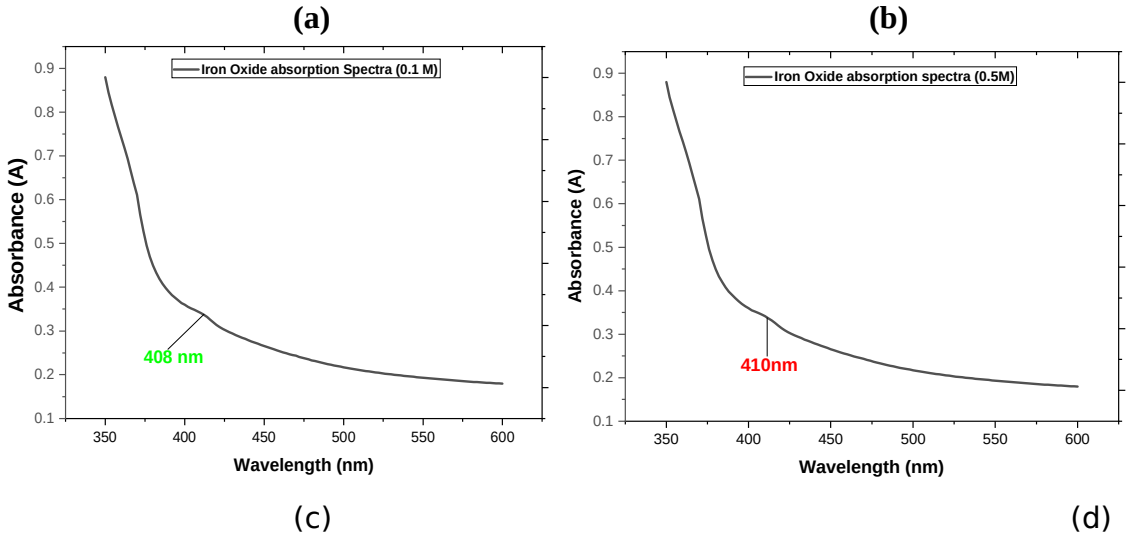

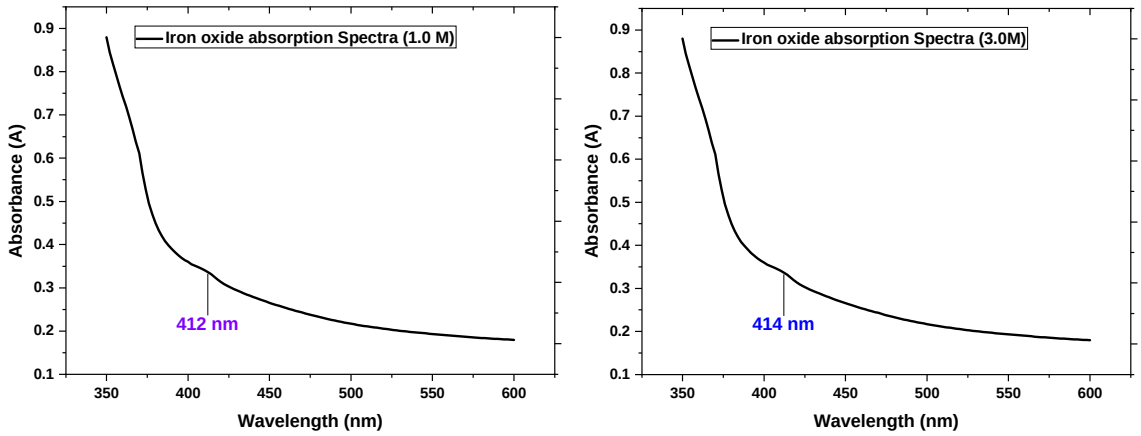

Figure 4.4: Iron Liberated: Absorbance Peaks of Iron Liberated at Respective Wavelengths.

The absorption spectra of the iron oxide were reported for the four different phosphoric acid concentration at 30 min time interval as indicated in **Tables (4.2-4.5).** Using the Beers Lambert law presented in chapter three, the iron concentration was computed. Standard Curves of iron concentration versus absorbance at 0.1 M, 0.5 M, 1.0 M, and 3.0M of the phosphoric acid solution are presented (**Figs. 4.5a-d**). These data (**Figs. 4.5a-d)** shows a linear dependency of concentration and absorbance as a function of time with their respective regression coefficients, R^2 values, indicating the goodness of fits for the linear model.

Table 4.2: Beer Lambert's relation for the absorbance and concentration of the iron oxide at 0.1 M phosphoric acid solution.

Leaching Duration (min)	**Iron Concentration (L/mol ×10^{-6})**	**Absorbance (Au)**
30	1.608	0.0337
60	2.843	0.0597
90	4.457	0.0936
120	7.567	0.1589

Table 4.3: Beer Lambert's relation for the absorbance and concentration of the iron oxide at 0.5 M phosphoric acid solution.

Leaching Duration (min)	Iron Concentration (L/mol ×10^{-6})	Absorbance (Au)
30	3.033	0.064
60	4.271	0.089
90	6.495	0.136
120	9.471	0.199

Table 4.4: Beer Lambert's relation for the absorbance and concentration of the iron oxide at 1.0 M phosphoric Acid solution.

Leaching Duration (min)	Iron Concentration (L/mol ×10^{-6})	Absorbance (Au)
30	4.667	0.0978
60	5.714	0.120
90	9.190	0.193
120	12.214	0.255

Table 4.5: Beer Lambert's relation for the absorbance and concentration of the iron oxide at 3.0 M phosphoric Acid solution.

Leaching Duration (min)	Iron Concentration (L/mol ×10^{-6})	Absorbance (Au)
30	8.333	0.175
60	9.429	0.198
90	10.619	0.210
120	16.643	0.345

(a)

(b)

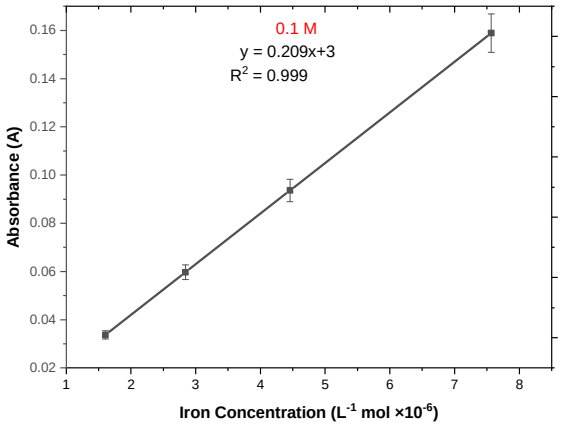
0.1 M
y = 0.209x+3
R2 = 0.999
Absorbance (A)
Iron Concentration (L-1 mol ×10-6)

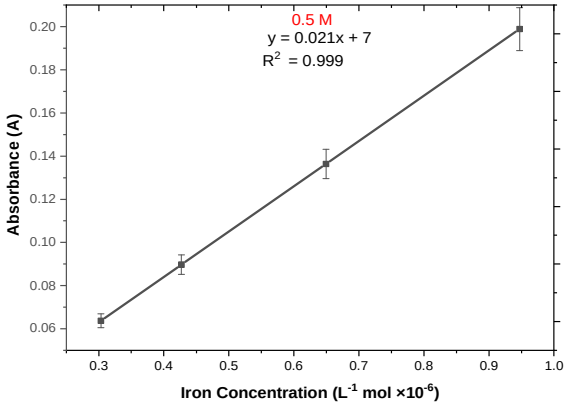
0.5 M
y = 0.021x + 7
R2 = 0.999
Absorbance (A)
Iron Concentration (L-1 mol ×10-6)

(c)

(d)

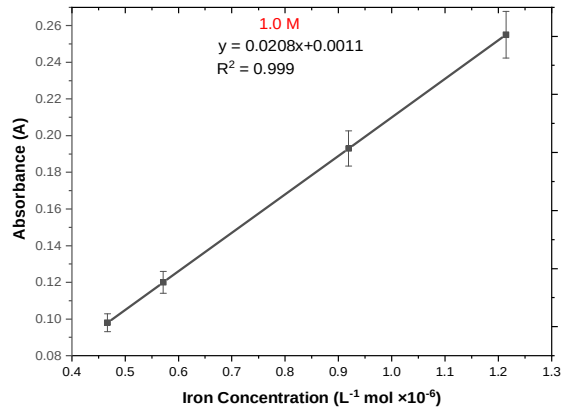

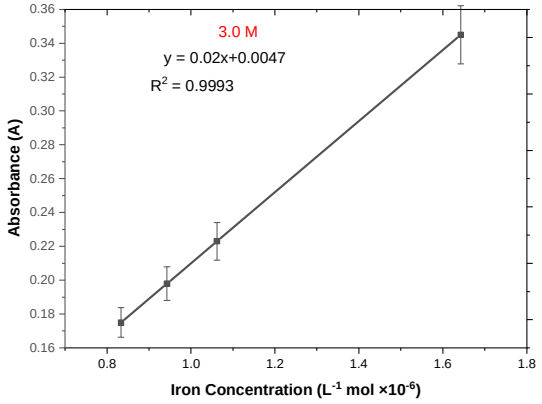

Figure 4.5: Standard Curve of Iron Concentration Versus Absorbance at: (a) 0.1 M, (b) 0.5 M, (c) 1.0 M, and (d) 3.0M Phosphoric Acid Solution.

4.3 Kinetics of Iron Release

In other to understand the kinetics of iron released, the zeroth-order, first-order, second-order, and Higuchi models were investigated in chapter three. **Table 4.6-4.9** showed the calculated concentrations (C), Ln(C), and inverse (C) for 0.1 M. Similar calculation have been done for all the concentration of phosphoric acid used in the experiment (i.e. 0.1 M, 0.5 M, 1.0 M, and 3 M). The reaction kinetics between 0.1 M phosphoric acid and iron dissolution is represented (**Figs. 4.6**) for zeroth order, first-order, second-order, and Higuchi model.

The results (**Fig. 4.6a-d**) has demonstrated the graphical fitting of the data to the models. The regression coefficient R^2 was used to ascertain the goodness of fit to the model. The model's presented shows that the reaction between 0.1 M phosphoric acid solution and iron follows the Higuchi Model of kinetic release in **Fig. 4.6 (d)**. The Higuchi model gave a regression coefficient, $R^2 = 0.996$. 0.5 M Phosphoric acid solution and the iron reaction is favoured by both the Higuchi Model of kinetic release and First-order reaction in **Fig. 4.7**. They have the same regression coefficient value, $R^2 = 0.804$. 1.0 M is favoured by the first-order reaction in **Fig. 4.8 (b)** and 3.0 M is favoured by the Higuchi model in **Fig. 4.9 (d).**

Table 4.6: Reaction kinetics between 0.1 M phosphoric acid and iron dissolution.

Time Interval (min)	**Square Root of time $(min)^{0.5}$**	**Iron Concentration (C) $(L/mol \times 10^{-6})$**	**Ln(C) $(L/mol \times 10^{-6})$**	$\frac{1}{(C)}$ **$(L/mol \times 10^{-6})^{-1}$**
0	0	7.567	2.0238	0.4941
30	5.477	4.457	1.4945	0.6691
60	7.746	2.843	1.0449	0.9571
90	9.847	1.608	0.4750	2.1053
120	10.954	0.546	0.2086	4.7941

Table 4.7: Reaction kinetics between 0.5 M phosphoric acid and iron dissolution.

Time Interval (min)	**Square Root of time $(min)^{0.5}$**	**Iron Concentration (C) $(L/mol \times 10^{-6})$**	**Ln(C) $(L/mol \times 10^{-6})$**	$\frac{1}{(C)}$ **$(L/mol \times 10\text{-}^{6})^{-1}$**
0	0	9.471	2.2428	0.4448

30	5.477	4.271	1.4518	0.6888
60	7.746	6.495	1.8710	0.5344
90	9.847	3.033	1.1096	0.9013
120	10.954	1.423	0.3528	0.8347

Table 4.8: Reaction kinetics between 1.0 M phosphoric acid and iron dissolution.

Time Interval (min)	**Square Root of time (min)$^{0.5}$**	**Iron Concentration (C) (L/mol ×10^{-6})**	**Ln(C) (L/mol ×10^{-6})**	$\frac{1}{(C)}$ **(L/mol ×10^{-6})$^{-1}$**
0	0	12.214	2.5026	0.3995
30	5.477	9.190	2.2181	0.4508
60	7.746	5.714	1.7429	0.5738
90	9.847	4.667	1.5405	0.6491
120	10.954	2.890	1.0613	0.9422

Table 4.9: Reaction kinetics between 3.0 M phosphoric acid and iron dissolution.

Time Interval (min)	**Square Root of time (min)$^{0.5}$**	**Iron Concentration (C) (L/mol ×10^{-6})**	**Ln(C) (L/mol ×10^{-6})**	$\frac{1}{(C)}$ **(L/mol ×10^{-6}) $^{-1}$**
0	0	16.643	2.812	0.3556
30	5.477	10.619	2.3626	0.4233
60	7.746	9.429	2.2438	0.4457
90	9.847	8.333	2.1202	0.4716
120	10.954	6.543	1.2947	0.7724

(a)

(b)

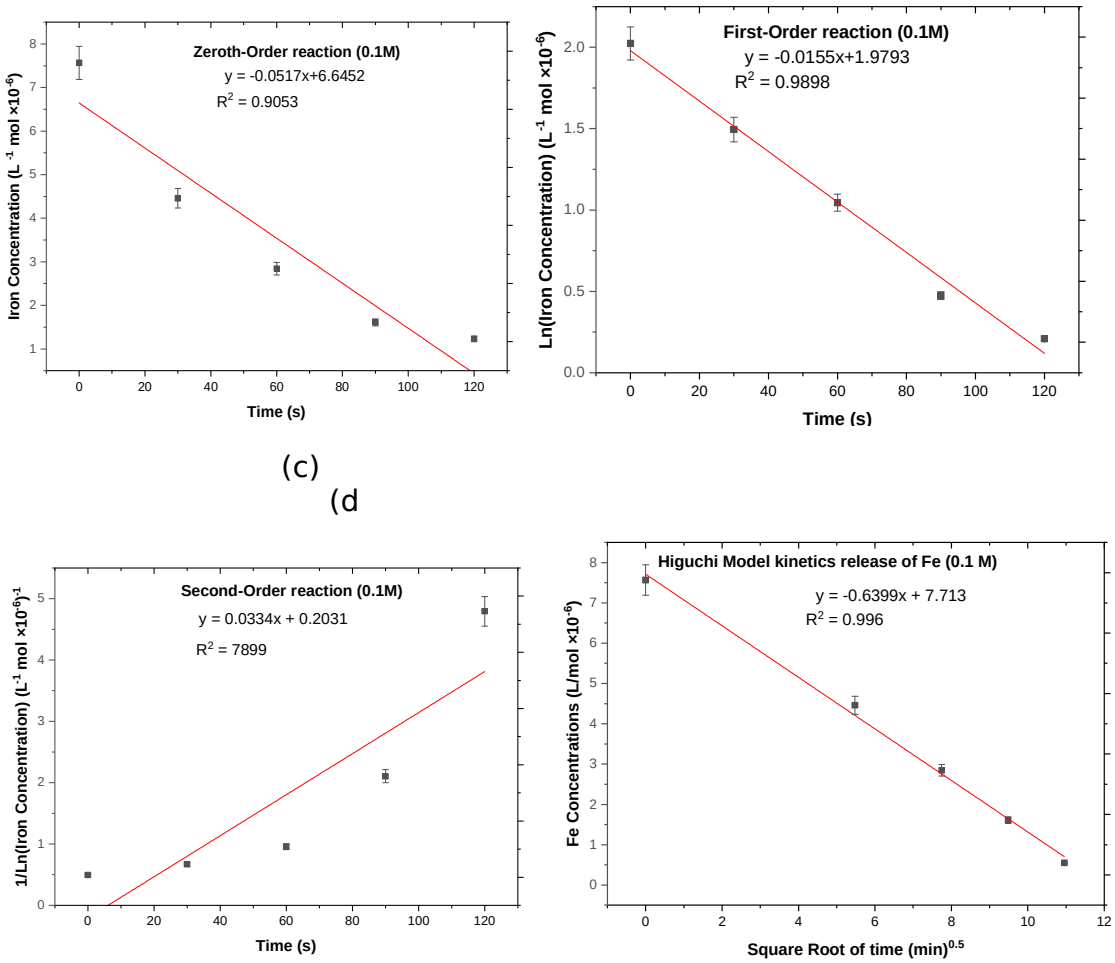

Figure 4.6: Verification of Zeroth, First, Second-order reaction and Higuchi Model for 0.1 M phosphoric acid solution.

(a)

(b)

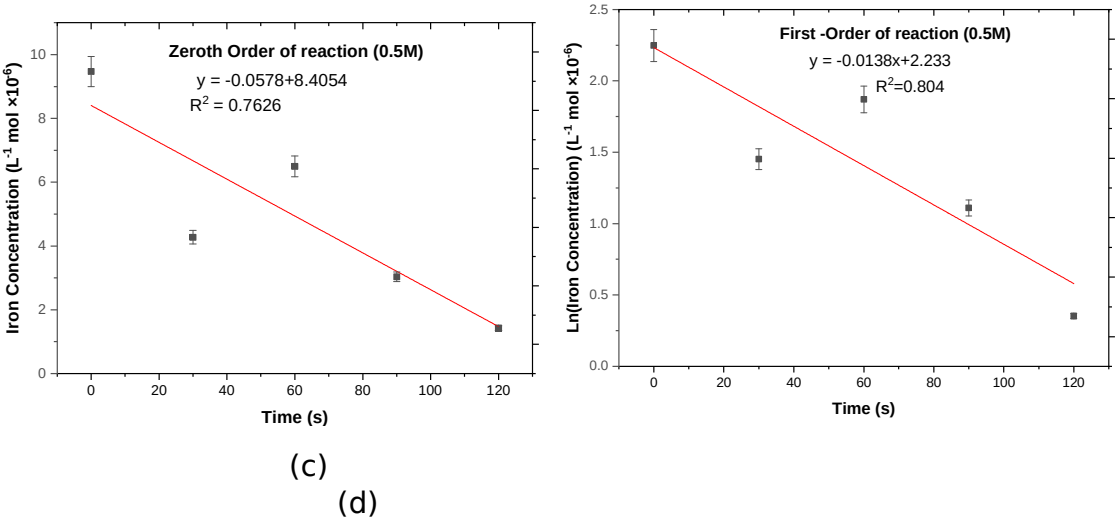

(c)

(d)

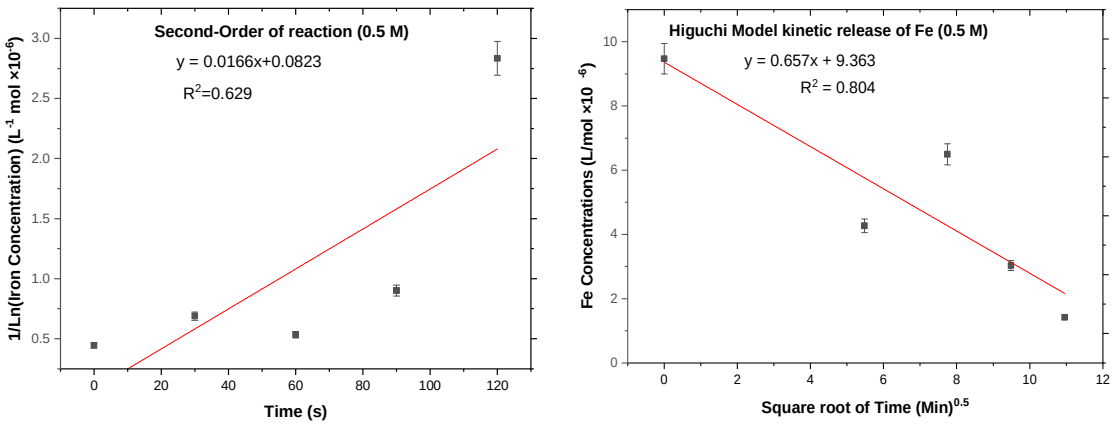

Figure 4.7: Verification of Zeroth, First, Second-order reaction and Higuchi Model for 0.5 M phosphoric acid solution.

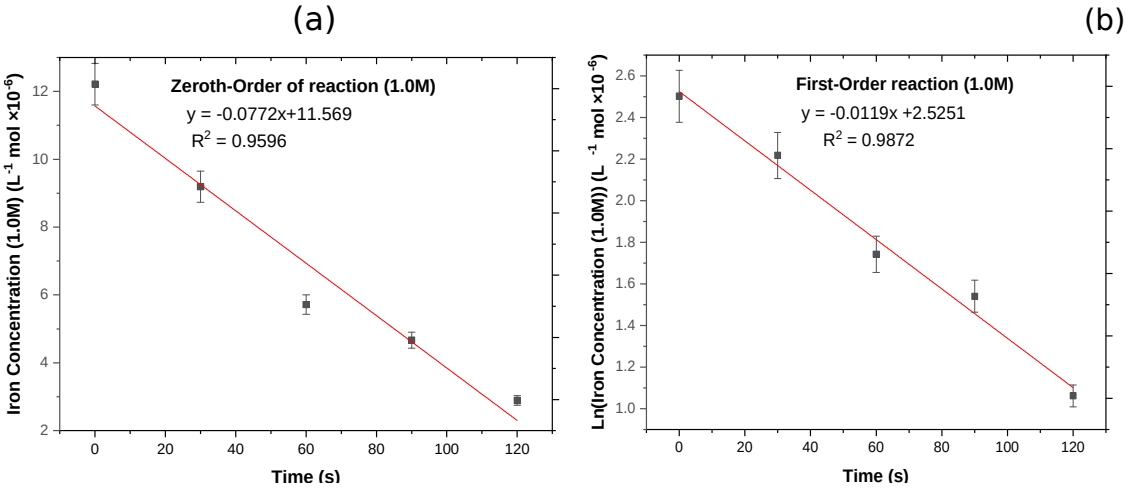

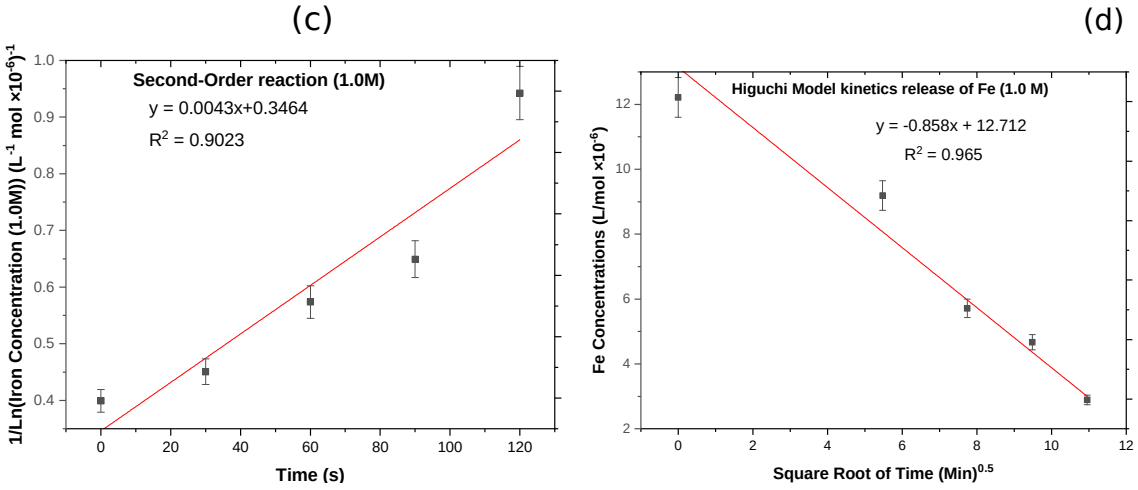

Figure 4.8: Verification of Zeroth, First, Second-order reaction and Higuchi Model for 1.0 M M phosphoric acid solution.

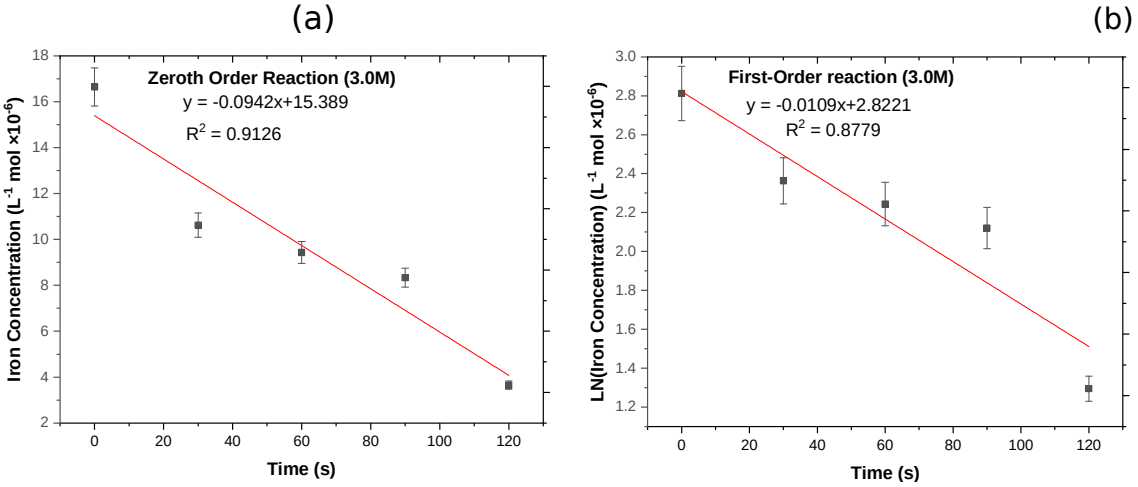

(c)

(d)

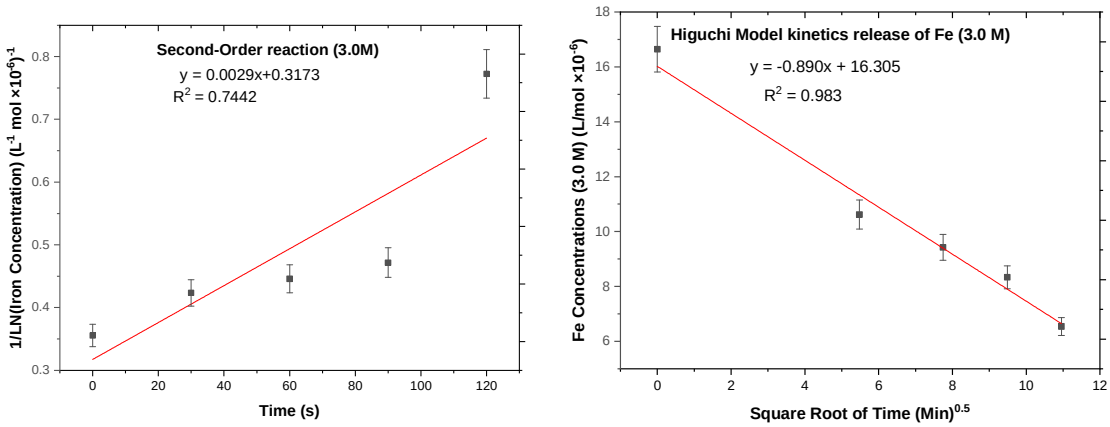

Figure 4.9: Verification of Zeroth, First, Second-order reaction and Higuchi Model for 1.0 M phosphoric acid solution.

4.4 Effect of Acid Concentration on the Dissolution of Iron.

EDS characterization shows the effect of iron leached as a function of residence time and phosphoric acid concentration **(Table 4.10)** and a corresponding graphical representation is presented in **Figure** (**4.10**). An increase in phosphoric acid concentration from 0.1 M to 3.0 M has caused a linear increase in the amount of iron liberated. Thus, increasing "phosphoric acid concentration increases the iron (Fe) dissolution rate in the clay sample". "It was observed that the leaching rate of Fe at 1.0 M was higher than that at 0.10 M" with Fe extractions at 6.71% and 1.48%, respectively. Also, 3.0 M was higher than 0.5 M with Fe percentage of 13.31% and, 4.44% respectively. The results also present the kinetics of iron leached when there is an increase in residence time of iron ore in solution. Thus, a prolonged interaction of clay impregnated iron ores with the phosphoric acid helped to liberate the iron into solution from 0 to 120 min. The result is in agreement with previous studies **[8]** where iron leaching was obtained from quartz sand as the raw material using phosphoric acid. This

phenomenon is observed as the reddish colour transforms into a white-coloured sample as shown **(Fig. 4.11).**

Table 4.10*:* Percentage of Iron leached at each time interval.

Time (Min)ED	**Measured Iron (Fe) content in the clay sample (%)**			
0	3.0 M	1.0 M	0.5 M	0.1 M
30	11.23	4.76	1.89	0.57
60	12.45	6.30	3.66	0.89
90	14.53	7.11	5.44	1.67
120	15.03	8.67	6.76	2.78
Average	**13.31**	**6.71**	**4.44**	**1.48**

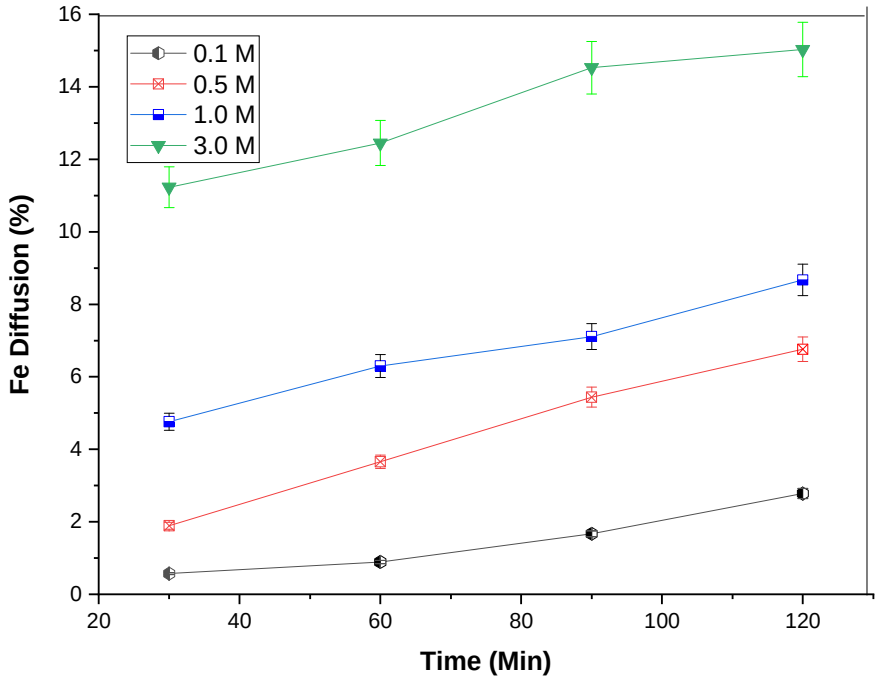

Figure 4.10: Effects of phosphoric acid molar concentration (0.1, 0.5 M, 1.0 M and 3.0 M) in Fe diffusion through time (30, 60, 90, and 120 min) at 100 ℃.

Figure 4.11: Initial Redish color of the clay sample turns to white after the leaching process.

4.5 Discussion

Phosphoric acid was used due to its theoretical advantage as compared to other inorganic acids [9]. Hydrogen ions play an important role in the leaching process in terms of dissolving the iron oxide from the sample. The phosphoric acid reagent provides the hydrogen ion to react with the iron oxide according to Zhanta et al **[3, 4].**

The reaction proceeds as follows:

$$6H^{+}+Fe_2O_3 \rightarrow 2Fe^{3+} +3H_2O \qquad (4.2)$$

The “activated surface of the iron oxyhydroxide species on the right-hand” side of **Equation (4.7)** adsorbed the hydrogen ions. Thus, “Hydrogen ions are adsorbed on the solid surface site and form the surface of the active center where the main reaction of dissolution” occurs. As the concentration of “hydrogen ions in the solution increases, the amount of hydrogen adsorbed by iron increases according to the adsorption principle”

[9]. An “increase in the number of active centres results in a corresponding increase in the dissolution rate” **[3,5].**

Additionally, the phosphoric acid reagent produce $PO_4^{3-¿¿}$ ions as the $H^{+¿¿}$ionizes. The phosphate has a “complexing ability to iron ions. All these features lead to the high leaching ability of H_3PO_4 acid”. This reaction may proceed according to Zhang et al. **[3,4].**

$$8\,H^{+¿}+4\,PO_4^{3-¿}+Fe_2O_3 \rightarrow [Fe(HPO_4)_2]^{-¿+[Fe(PO_4)_2]^{3-}+3H_2O¿}{}_{¿}{}_{¿} \qquad (4.3)$$

The multiple reactions of phosphoric acid lead to high leaching ability.

Synthesizing iron oxides particle via chemical leaching was demonstrated. The iron diffused out of the clay sample due to the reducing ability of the phosphoric acid used. Basic theoretical computation was used to demonstrate how the phosphoric acid reacted with the sample and the diffusion through the product layer using the heterogenous shrinking core model.

Electron Dispersive spectroscopy investigation gave 16.8% iron present in the clay sample before the leaching experiment was carried out. After the leaching, using different concentrations of the acid at different time interval another EDS data was obtained. This gave a reduced percentage of the iron as illustrated in **Table 4.1.** This result is further confirmed as the initial reddish colour changed to whitish studied previously **[9]**.

Fourier Transform Infrared Spectroscopy techniques were used to analyze the chemical bonds associated with the clay minerals. The results obtained were similar to other previous studies **[9, 10].** The Filtrate was characterized using UV/Vis spectroscopy.

The four sets of concentrations gave absorption spectra at 408, 410, 412 and 414 nm as shown in **Figure 4.4.**

References

[1] M. Balamurugan, S. Saravanan, and T. Soga, "Synthesis of iron oxide nanoparticles by using eucalyptus globulus plant extract," *e-Journal Surf. Sci. Nanotechnol.*, vol. 12, no. August, pp. 363-367, 2014. DOI: 10.1380/ejssnt.2014.363.

[2] S. S. Behera, J. K. Patra, K. Pramanik, N. Panda, and H. Thatoi, "Characterization and Evaluation of Antibacterial Activities of Chemically Synthesized Iron Oxide Nanoparticles," *World J. Nano Sci. Eng.*, vol. 02, no. 04, pRep. 196-200, 2012. Doi: 10.4236/wjnse.2012.24026.

[3] U. P. Acid, "Kinetics of Iron Leaching from Kaolinitic Clay, Using Phosphoric Acid," 2016. DOI: 10.3390/min6030060.

[4] T. Zhang, Z.; Li, J.; Li, X.; Huang, H.; Zhou, L.; Xiong, "High-efficiency iron removal from quartz sand using phosphoric acid," *Int. J. Miner. Process. Miner. Process.*, vol. 114, pp. 30-34, 2015.

[5] F. H. Norton, "Fine Ceramics: Technology and Applications;" Robert, E., Ed.; Krieger Publ. Co. New York NY, USA, 1978.

[6] F. L. Guimares, S.J.F.; De Olivera, N.; De Salles, "Purification of registro kaolin by magnetic separation.," *Trans. Inst. Min Met.*, no. 51, pp. 13-17, 2003.

[7] M. E. Sohn, H.Y.; Wadsworth, "Rate Processes of Extractive Metallurgy;," Springer Boston, MA, USA, 1979.

[8] P. C. Saikia, N.J.; Bharali, D.J.; Sengupta, P.; Bordoloi, D.; Goswamee, R.L.; Saikia, P.C.; Borthakur, "Characterization, beneficiation and utilization of a kaolinite clay from Assam," *India. Appl. Clay Sci.*, vol. 24, pp. 93-103, 2014.

[9] S. K. Suman and S. Kumar, "Reverse flotation studies on iron ore slime by the synergistic effect of cationic collectors," *Sep. Sci. Technol.*, vol. 55, no. 9, pp. 1702-1714, 2020. Doi: 10.1080/01496395.2019.1604757.

[10] P. Karpagavinayagam and C. Vedhi, "SC," *Vacuum*, 2018, DOI: 10.1016/j.vacuum.2018.11.043.

[11] G. Jagathesan and P. Rajiv, "Biocatalysis and Agricultural Biotechnology Biosynthesis and characterization of iron oxide nanoparticles using Eichhornia

crassipes leaf extract and assessing their antibacterial activity," *Biocatal. Agric. Biotechnol.*, vol. 13, 2017, pp. 90-94, 2018. DOI: 10.1016/j.bcab.2017.11.014.

[12] H. K. Shaikh, R.V. Kshirsagar, S.G. Patil. Mathematical models for drug release characterization: A review. World Journal of pharmacy and pharmaceutical sciences. Vol. 4(4) (2015) 324-338, 2017.

CHAPTER FIVE

5.0 CONCLUSIONS AND RECOMMENDATIONS FOR FUTURE WORK

5.1 Conclusions

In this work, iron oxide in the range of microns was investigated from a bioinspired termite mound via leaching with phosphoric acid. The synthesized iron oxide was analyzed by FT-IR, UV-Vis Spectroscopy, EDS and SEM.

Leaching of iron with phosphoric acid solutions at acid concentration and time was more effective. Dissolution of iron was significant at 100ºC and 120 min duration, at which 14.53% of Fe were removed. The results of this study indicate that leaching of iron occurs by diffusion through the product layer.

It was observed that as the Molarity of the acid increases, the diffusion of iron Fe from the clay sample increases.

UV-Vis was conducted to confirm the formation of the iron oxide in the solution. The UV-Vis spectroscopy spectra of the particles displaced absorbance within 350-600 nm wavelength range which is in agreement with the literature for the "production of the magnetic iron oxide nanoparticles". A distinct peak was observed at $412\,nm$ which is in agreement with the literature.

EDS was conducted to confirm the formation of the iron oxide by analysing, for the presence of Iron (Fe) and Oxygen (O) in the sample. EDS data proved the existence of iron (Fe) and oxygen (O) in the produced particles. In addition, it showed the presence of other elements which include silicon (Si), phosphorus (P) and aluminium (Al). The presence of phosphorus found in the particles was attributed to the elemental complexity of the acid solution employed during the synthesis.

FTIR was conducted to confirm the presence of the Fe-O to indicate the formation of the Iron oxide being synthesized.

SEM images revealed high levels of particles agglomeration. Some of the particles showed very high levels of agglomeration compared with others. The morphology of the particles cannot be clearly defined in most of the samples due to this reason. However, the results show particles with multi-shapes that can produce different levels of magnetizations and hence can support laser applications in which localized hyperthermia could be employed in the near future to support cancer treatment.

5.2 Recommendation for Future Work

Further Analysis could be conducted to confirm the formation of Iron oxide Nanoparticles (IONPs) and safer ways of precipitating these IONPs from the filtrate. Chemical and structure analysis using XRF and XRD, respectively could be used to determine the oxide composition and the structure of the IONPs.

Transmission Electron Microscopy (TEM) could be used to investigate the IONPs particle size and morphology.

The IONPs could be functionalized with molecular recognition unit for an *in-vitro* experiment. Future work could be done to investigate the effect of the IONPs particle size.

IONPs in their applications have usually composed of a magnetic core engulfed with various functional groups which could aid hyperthermia treatment, magnetic resonance imaging (MRI), optical imaging, biosensor, and cell separation. IONPs could be directed to particular cancer sites for targeted and localized drug delivery using an external magnetic field in cancer treatment. Also, in the detection of cancer growth, they can be scanned with MRI's when developed and designed by embedding them with receptors that would attract them to the cancer cell. When synthesized and functionalized, they would offer potential therapeutic effects on cancer cells.

Reference

[1] U. P. Acid, "Kinetics of Iron Leaching from Kaolinitic Clay, Using Phosphoric Acid," 2016, DOI: 10.3390/min6030060.